

**2D RESISTIVITY INVESTIGATION OF CASSITERITE (TIN ORE) BEARING
LAYER AT PINGEL VILLAGE, MAGAMA GUMAU, BAUCHI STATE, NIGERIA.**

BY

BASHIR, OGIRMA YUSUF

**DEPARTMENT OF PHYSICS,
FACULTY OF SCIENCE
AHMADU BELLO UNIVERSITY,
ZARIA, NIGERIA**

MAY, 2021

**2D RESISTIVITY INVESTIGATION OF CASSITERITE (TIN ORE) BEARING
LAYER AT PINGEL VILLAGE, MAGAMA GUMAU, BAUCHI STATE, NIGERIA.**

BY

BASHIR, OGIRMA YUSUF

P18SCP8323

SUPERVISORY COMMITTEE

Dr. RAIMI JIMOH

Dr. A.L. AHMED

**A DISSERTATION SUBMITTED TO THE SCHOOL OF POSTGRADUATE
STUDIES AHMADU BELLO UNIVERSITY IN PARTIAL FULFILLMENT OF
THE REQUIREMENT FOR THE AWARD OF A
MASTER DEGREE IN APPLIED GEOPHYSICS**

**DEPARTMENT OF PHYSICS,
FACULTY OF SCIENCE,
AHMADU BELLO UNIVERSITY,
ZARIA, NIGERIA**

MAY, 2021

DECLARATION

I declare that the work in this thesis entitle “2D resistivity investigation of cassiterite (tin ore) bearing layer at Pingel Village, MagamaGumau, Bauchi State, Nigeria.” has been carried out by me in the Department of physics. The information derived from the literaturehas been duly acknowledged in the text and a list of references provided. No part of this thesis was previously presented for another degree at this or any other institution.

BashirOgirma YUSUF

Name of student

Signature

Date

CERTIFICATION

This dissertation entitled “2D resistivity investigation of cassiterite (tin ore) bearing layer at Pingel village, MagamaGumau, Bauchi State, Nigeria” by BashirOgirmaYUSUF meets the regulations governing the award of Masters of Science in Applied Geophysics of the Ahmadu Bello University, and is approved for its contribution to knowledge and literary presentation.

Dr. RaimiJimoh

(Chairman, supervisory Committee)

Signature

Date

Dr. A. L Ahmed

(Member, supervisory Committee)

Signature

Date

Prof. NasiruRabiu

(Head of Department)

Signature

Date

Prof. SaniAbdullahi

(Dean Postgraduate School)

Signature

Date

DEDICATION

This work is dedicated to Almighty Allah, The universal source of all Knowledge, Wisdom and Understanding.

ACKNOWLEDGEMENT

I wish to acknowledge the guidance of Almighty Allah, who by his infinite mercy and love, kept me alive in sound health through this resourceful and promising research work.

I seize this opportunity to express my profound gratitude to my kindhearted supervisor Dr. Raimi Jimoh, who despite his tight schedules, read and reread this work several times, making strong criticisms and kind advice that led to the successful completion of this work. May Almighty Allah continue to shower him more blessing and see him through in all his endeavors. (Amen)

My sincere thanks and appreciation also go to my amiable, diligent second supervisor Dr. A. L. Ahmed for his easy going and always approachable attitude to me with numerous suggestions, constructive criticism, corrections and academic contributions in the course of this research. May Allah reward him accordingly. (Amen)

I am also grateful to Prof. K. M. Lawal who occasionally paid attention to my academic needs and offered some useful suggestions, contributions in various forms that led to the success of this work.

My special thanks go to the technical staff Alh. Ibrahim Sani assistance during the course of my fieldwork. May Allah reward him abundantly.

My thanks also go to my senior colleagues, Yusuf Anyoola, Abubakar Aliyu Shonga, Matthew Ogwuche, Daniel Eshimiakhe for their cordial relation and advice during the course of our programme.

My profound appreciation goes to my Parents, my siblings Capt. Z. Yusuf, Mrs. Nafisa Yusuf, Dr. Yusuf Ahmed, Eng. Yusuf Kabir, Miss Jummai Sheidu and Miss Aisha Obinifor their kind support throughout my studies.

I also want to thank my lovely wife Mrs. Umar Farouk Murjanatu and our lovely daughter for their love and support.

May Allah bless you all immensely.

ABSTRACT

Two dimensional geoelectric resistivity survey was conducted at the mining site in Pingel village, MagamaGumau, Bauchi state, Nigeria. The survey was undertaken to characterize the cassiterite bearing layer in the area. A test profile was conducted along a point with an exposed subsurface that reveals different layers of the earth, including that rich in cassiterite, to detect the best configuration to be used. Based on the result obtained from the test profile, the Schlumberger array proved to be a better representation of the layering of the study area. A total of five profiles were then taken and the result of the 2D resistivity survey revealed the occurrence of three to four layers in the geoelectric models. The top layer consists of earth materials with resistivity values mostly less than 120 Ωm , inferred to consist of mainly clayey sand and laterite with an approximate thickness of 4.5 m. The second layer has resistivity range of 60 Ωm to 250 Ωm and may consist of weathered and fracture rocks with cassiterite composition at approximately 7.0 m depth. The third layer is composed of highly resistive materials, generally greater than 800 Ωm , at a depth stretching beyond 7 m. The high resistivity values could be associated with the fresh basement.

TABLE OF CONTENTS

Cover page.....	i
Title Page.....	ii
DECLARATION	iii
CERTIFICATION.....	iv
DEDICATION	v
ACKNOWLEDGEMENT	vi
ABSTRACT	vii
TABLE OF CONTENTS	viii
LIST OF PLATES.....	xi
LIST OF TABLES	xii
LIST OF FIGURES	xiii
ABBREVIATION, AND SYMBOLS USED	xv
CHAPTER ONE	1
INTRODUCTION.....	1
1.1 General Background.....	1
1.2 Location, Climate and Vegetation of Study Area.....	3
1.3 Geology of Study Area.....	4
1.4 Statement of Research Problem	7
1.5 Justification	9
1.6 Aim and Objectives of the Study.....	10
CHAPTER TWO.....	11
LITERATURE REVIEW	11
2.1 Previous Works on Cassiterite Mineralization and Exploration.....	11
2.2 Tin Mineralization in Nigeria	13
2.2.1 Sn-Ta-Nb Pegmatite Belt of Late Pan-African age	14
2.2.2 Sn-Nb-Ta Younger Granite Province of Jurassic Age	17
2.2.3 The History of Tin Mining in Nigeria 1904 – 1960.....	18
2.3 Principle of the Electrical Resistivity Method	21
2.3.1 Theory of the Resistivity Method	24
2.4 Electrical Resistivity Configurations.....	29
2.4.1 Wenner Configuration	30

2.4.2 Schlumberger Configuration	31
2.4.3 Dipole-Dipole Configuration	33
2.5 Resistivity of Rocks, soil and Minerals.....	34
2.6 Factors Affecting Electrical Resistivity	36
2.6.1 Water Salinity.....	36
2.6.2 Porosity of Rock	37
2.6.3 Effect of Temperature.....	37
2.6.4 Effects of Rock Texture and Porosity.....	38
2.6.5 Effects of Geological Processes	38
CHAPTER THREE.....	39
MATERIALS AND METHOD	39
3.1 Instrumentation	39
3.1.2 ABEM LUNG Imaging System (SAS 1000).....	39
3.2 Field Work	41
3.2.1 Reconnaissance Survey	41
3.2.2 Data Acquisition	41
3.2.3 Field Problems	45
3.3 Data Processing Procedure	46
CHAPTER FOUR	52
RESULTS AND INTERPRETATION	52
4.1 Lithological Log.....	52
4.2 Inversion and Interpretation of 2D Model of ERT Data Acquired at Test Site	54
4.3 Inversion of Acquired 2D ERT Data	56
4.4.1 Result of Profile 1	56
4.4.2 Result of Profile 2	57
4.4.3 Result of Profile 3	58
4.4.4 Result of Profile 4	59
4.4.5 Result of Profile 5	59
CHAPTER FIVE.....	64
DISCUSSION, CONCLUSION AND RECOMMENDATION	64
5.1 Discussion	64
5.2 Conclusion.....	66
5.3 Recommendation	67

REFERENCES 68

LIST OF PLATES

Plate 1.1A, B: Artisanal minners digging samples from minning pits -----	8
Plate 3.1: Terameter and its Accessories -----	41

LIST OF TABLES

Table 3.1: Coordinates of Beginning and End Points of Each Profile -----	45
Table 4.1: Standard Resistivity Values of Rock Materials -----	51
Table 4.2 gives an overview of the profiles, showing the maximum and minimum resistivity and depth of each layer-----	61

LIST OF FIGURES

Figure 1.1: Location Map of Study Area-----	4
Figure 1.2: Geologic Map of the Study Area -----	7
Figure 2.1: Metallogenic Map of Nigeria -----	14
Figure 2.2: Map showing Location of Notable Tin-Bearing Pegmatites in Nigeria-----	16
Figure 2.3: Current Flow Lines and Equipotential Between Two Current Electrodes-----	22
Figure 2.4: 2D Data Collection Using Multielectrode Resistivity System -----	23
Figure 2.5: General Four Electrode Arrangement -----	29
Figure 2.6: The Wenner Configuration -----	31
Figure 2.7: The Schlumberger Configuration -----	32
Figure 2.8: The dipole- dipole Configuration -----	34
Figure 2.9: Resistivities of rock, soils and minerals-----	35
Figure 3.1: Profile layout superimposed on google earth map -----	43
Figure 3.2: Two possible arrangements of the blocks used in a 2-D model together with the data points in the pseudo-section-----	49
Figure 3.3: Profile showing data set with bad data points -----	51
Figure 4.1: Section of exposed subsurface in study area -----	53
Figure 4.2: Result of 2D Inversion of the dipole-dipole array with section along Test Profile-----	55

Figure 4.3: Result of 2D Inversion of the Wenner array with section along Test Profile-----	55
Figure 4.4: Result of 2D Inversion of Schlumberger array with section along Test Profile-----	56
Figure 4.5: Result of 2D Inversion of Schlumberger along profile 1-----	57
Figure 4.6: Result of 2D Inversion of Schlumberger along profile 2-----	58
Figure 4.7: Result of 2D Inversion of Schlumberger along profile 3-----	58
Figure 4.8: Result of 2D Inversion of Schlumberger along profile 4-----	59
Figure 4.9: Result of 2D Inversion of Schlumberger along profile 5-----	60
Figure 4.10: Spatial display of ERT of the study area-----	62
Figure 4.11: 3D horizontal depth slices of the subsurface with a grid size of 41x5-----	63

ABBREVIATION, AND SYMBOLS USED

VES	Vertical electric sounding
m	Meter
mm	Millimeter
km	Kilometer
mV	millivolt
V	volt
mA	milliampere
d.c.	Direct current
A.B.U.	Ahmadu Bello University
G.I.S.	Geographic information system
K_f	Geometric Factor
Ω	ohm
π	pi (= 3.142)
ρ	True resistivity
ρ_a	Apparent resistivity
MN	Potential electrode separation
AB	Current electrode separation

<i>i.e.</i>	That is
<i>et al.</i>	And others
E	Electric field
J	Current density
σ	Conductivity of the medium
U	Scalar potential function
∞	Infinity

CHAPTER ONE

INTRODUCTION

1.1 General Background

Tin is one of the metals known to mankind since the earliest times (Umeshwar, 2011; Kinnaird, 2016). It was possibly one of the first metals used by man as an ingredient of bronze (alloy of copper and tin). Bronze objects such as weapons, tools, jewelry, etc. with 10-14% tin have been found in excavations of different ancient civilization. A bronze rod found in Egypt has been dated back to 3700 B.C. Tin has also been found in the tomb of ancient Egyptians and was exported to Europe in large quantities from Cornwall, England during the Roman period (Umeshwar, 2011).

Tin has been mined and used in Nigeria as early as the 9th century with exquisite bronze artifacts from three sites in the Igbo-Ukwu area of Anambra State dating back to this period. These artifacts are older than the earliest Benin bronzes, which are dated to the 13th century (Kinnaird, 2016). Tin is a relatively soft, ductile metal with a silvery white color. Tin finds industrial applications in the production of corrosion-resistant alloys (bronze, brass, solder), tin plates, chemicals, tin foil, pottery, and glass. Although tin is usually a minor constituent in alloys, it is an essential one on account of the way in which its special properties confer improvements to the matrix metal.

Cassiterite, stannite and cylindrite are the major ore minerals of tin. Tin ores occur mainly in veins, stockworks, disseminations, pegmatites, replacements and placers. Primary tin deposits are formed by magmatic, hydrothermal and/or replacement processes. Secondary deposits are the products of weathering of primary deposits, and the subsequent transportation and deposition of the resulting sediments in a new environment.

Tin deposits are abundant in China, Malaysia, Indonesia, Peru, Thailand, Brazil, Bolivia, D.R. Congo, Australia, Nigeria, Myanmar (Burma), Russia, Zimbabwe, Rwanda, South Africa, United Kingdom, Mongolia, Colombia, Germany, Canada, Mexico and Morocco (Sainsbury, 1969; Olade, 1980; Carlin, 2012; International tin research Ltd., 2016). The estimated total world reserve of tin metal as at 2017 is over 4.80 million tonnes and global production amounted to 290,000 tonnes with China being the largest producer (100,000 tonnes) and Nigeria contributing about 2,400 tonnes (U.S. Geological survey, 2018). About 80% of tin mined in Nigeria is from secondary deposits found downstream (tin placer deposits) derived from primary tin lodes and granitic rocks (Imeokparia, 2015).

Geophysics is a discipline that gives information about the earth's subsurface without necessarily indulging in the invasive digging of the earth's surface. Its survey involves measuring the physical properties of the ground (or structure) to determine any variations (anomalies) in the background readings. Occurrence of anomalies can indicate presence of feature or changes in materials composition. It has been used for environmental, geotechnical and mineral exploration. For geophysical technique to be useful in mineral exploration, contrast must exist in the physical properties of the rocks concerned that are related directly or indirectly to the presence of economically significant mineral. Also, the suitability of a method depends on the sites' peculiar conditions and the composition of target features. There are a wide range of geophysical methods which have found relevance in many areas such as ground water investigation, mineral exploration, oil and gas prospecting, engineering site investigation and geothermal exploration. Some of these methods are the seismic, Magnetic and Electrical resistivity methods. Each of these methods is sensitive to physical property and features of earth materials. For the purpose of

this research, Electrical resistivity method was used to characterize cassiterite (tin ore) bearing layer in MagamaGumau-Pingel, Toro local government, Bauchi state, Nigeria. This technique has been chosen because it has proven successful in identifying earth materials with metallic composition, on the basis of resistivity contrast that exist between tin ore deposit and surrounding formation (Saad *et al*, 2012).

Electrical imaging surveys are now widely used to map areas with complex subsurface geology. The many applications include groundwater exploration, mineral exploration, environmental and engineering studies (Dahlin, 1996; Griffiths and Barker, 1993). Resistivity surveys determine the variation in the electrical resistivity of the subsurface by applying electric current across arrays of surface electrodes (Loke, 1999). Electrical resistivity is a function of porosity, fluid saturation, resistivity of the pore fluid and the solid, and the material texture among others. The survey data are processed to produce graphic depth sections of the thickness and resistivity of the subsurface electrical layers. All resistivity methods employ an artificial source of current, which is introduced into the ground through point electrodes or long line contacts; the latter arrangement is rarely used nowadays. The procedure is to measure potentials at other electrodes in the vicinity of the current flow. Because the current is measured as well, it is possible to determine an effective or apparent resistivity of the subsurface (Telford *et al.*, 1990).

1.2 Location, Climate and Vegetation of Study Area

The study area is situated in Pingel village, Toro local government area of Bauchi state Nigeria (Figure 1.1); Along Bauchi-Zaria road. Its geographical coordinates are Latitude $10^{\circ} 20' 00''$ N to $10^{\circ} 22' 00''$ N and Longitude $9^{\circ} 5' 00''$ E to $9^{\circ} 7' 00''$ E (See Figure 1.1).

The area is characterized by two seasons, wet and dry. The wet season lasts between April and October, with August having the highest precipitation while the dry season extends from November to March. The temperatures generally fall in July and August periods of the year corresponding to the peak of rainy season, as well as in December and January periods corresponding to the peak of harmattan in the area. The vegetation here is that of Sudan Savannah characterized by grasses, shrubs, thorns and scattered trees.

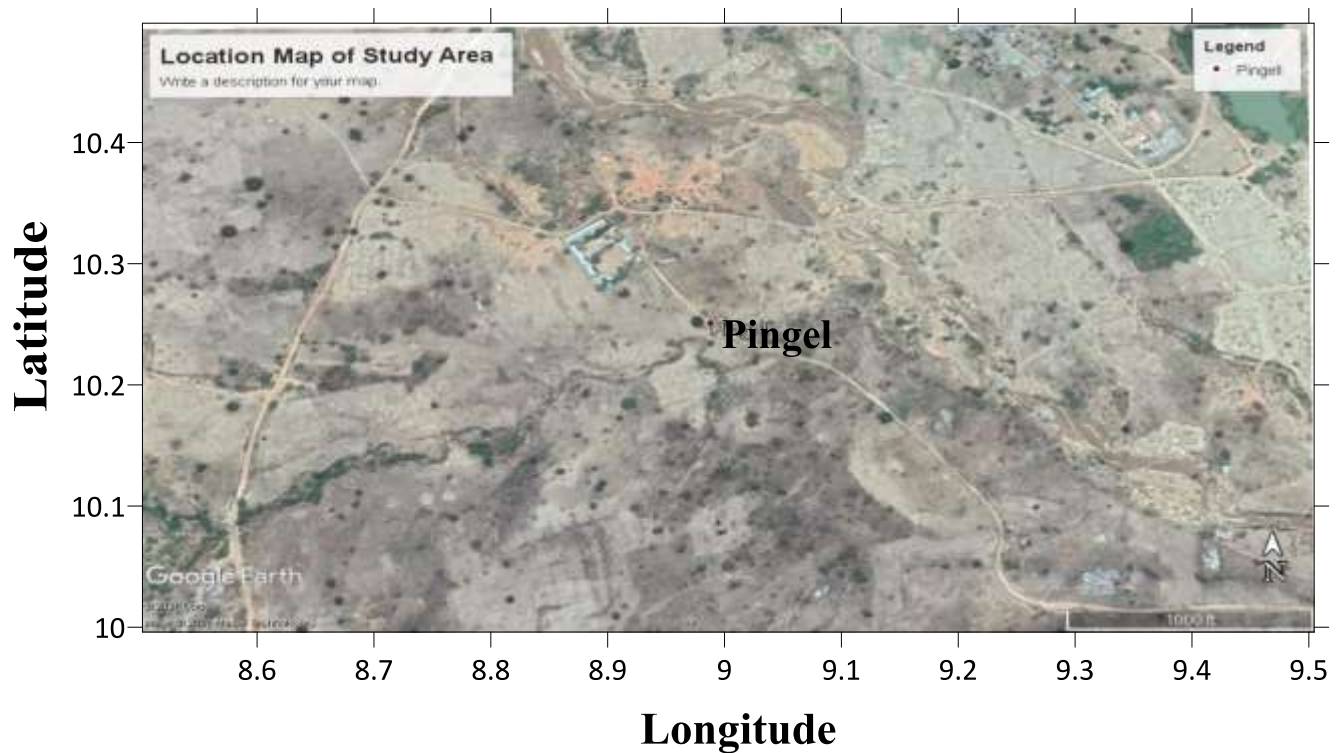


Figure 1.1: Location map of the study area.(Source: Google map)

1.3 Geology of Study Area

The study area, which is situated at the Younger granite province, is intruded into an undifferentiated amphibolite grade basement composed of migmatites and granitic gneisses (Ajakaiye, 1974). Three major igneous units common to the Younger Granite suite make up the exposure and exhibit sharp mutual contacts (Raeburn *et al.*, 1927; Turner, 1972;

Jacobson and MacLeod, 1977). In chronological order these are volcanics, biotite granite and albite riebeckite granite. Remnants of an initial volcanic phase are preserved as a narrow outcrop of explosion breccia 600 m long and up to 60 m wide composed entirely of basement rock fragments up to 0.3 m in diameter along the southern flank of the complex (Jacobson and MacLeod, 1977). The main intrusive forms 80% of the exposed complex and is nonporphyritic fine- to medium-grained biotite granite which has a homogeneous macroscopic texture and composition (Jacobson and MacLeod, 1977). Its well-developed north-northwest joint system controls drainage in the immediate vicinity of its outcrop (Ajakaiye, 1977). The most prominent of these lineaments occurs as a broad steep-sided flat-bottomed valley up to 1 km wide containing an underfit stream which drains to the northwest from the central part of the biotite granite exposure. Preliminary interpretation of aerial photographs of this feature suggests that it may be a fault or shear zone (Ajakaiye, 1977).

The biotite granite is the source rock for the tin deposits mined on a very small scale in the area although Raeburn et al. (1927) noted that the complex exhibited excessive tin mineralization for its outcrop size. Tin deposits are typically associated with biotite granite throughout the Younger Granite Province.

A later intrusion of albite riebeckite granite, which is somewhat arcuate and poorly exposed, flanks the biotite granite on its east side. It is extremely variable in texture but is compositionally homogeneous except in the degree of late stage albitization (Jacobson and MacLeod, 1977). Contacts with the basement rocks to the east are poorly defined. Remnants of aegerine commonly form the cores of riebeckite grains. Several felsitic dikes (mostly biotite microgranites) associated with the biotite granite (Jacobson and MacLeod,

1977) cut the granite as well as basement rocks adjacent to the southern and eastern margins of the complex.

The sequence of extrusive and intrusive igneous events in the province is well documented (Turner, 1963, 1972) and consists of an initial predominantly acidic volcanic phase accompanied or immediately followed by the formation of a peripheral vertical-sided ring fracture which broke the surface and which was filled, in most cases, with granite porphyry upon subsidence of the rock's interior to the ring fracture. A long waning felsic intrusive phase followed. In the case of the study area, the present outcrop limits give the probable extent of the associated initial ring fracture. Ring fracture followed by cauldron subsidence is considered to be the major mode of intrusive emplacement for the Younger Granites and is thought to give rise to plutons roughly circular in plan with generally steeply dipping contacts (Turner, 1963, 1972; Black and Girod, 1973; Jacobson and MacLeod, 1977). Studies by Billings (1945) in New Hampshire indicate that ring fractures may result from vertical extension caused by the upward directed pressure of an upwelling magma. Richey (1928) suggested a similar process for ring fracture formation in Northern Ireland. Once ring fractures are created ring dikes can be produced by cauldron subsidence, block or piecemeal stopping (Billings, 1945), reduction of magma chamber pressure to produce settling of the central block (Anderson, 1936) or upward removal of host-rock debris within the fracture by gas coring or volcanic activity (Turner, 1963). Figure (1.2) is the geological map of the study area and environs showing the various rock units.

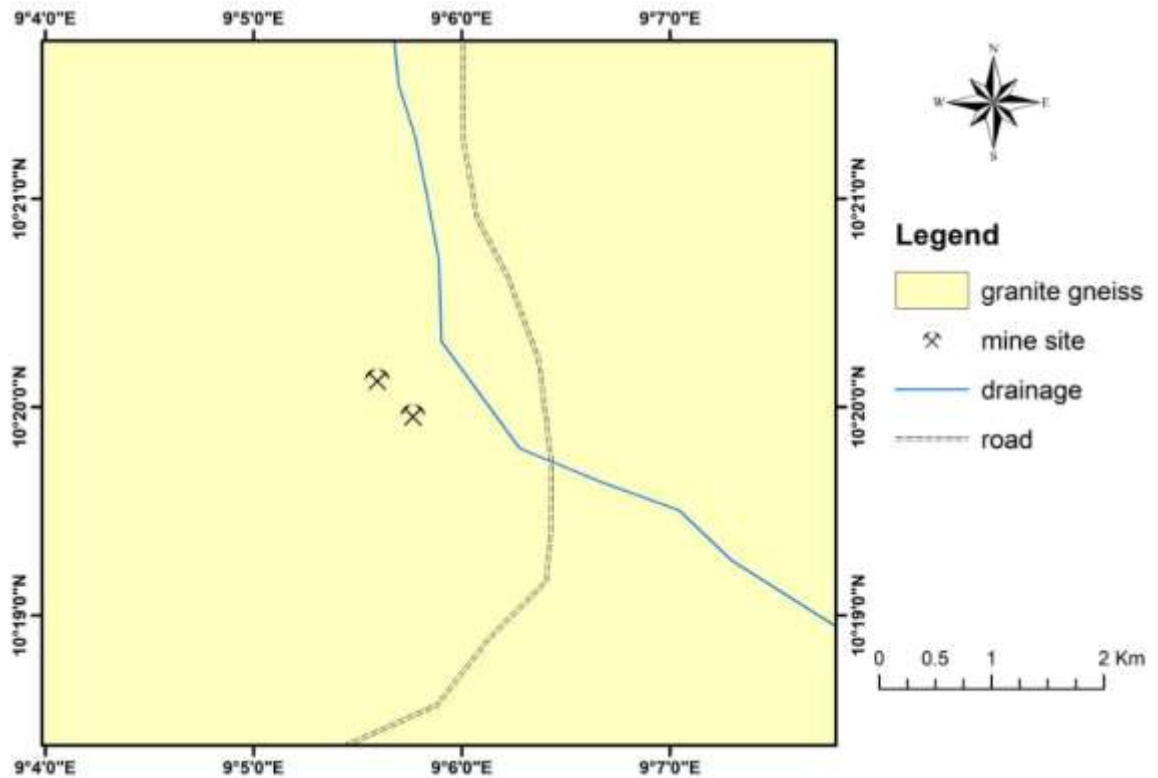


Figure 1.2: Geological Map of the Study Area. (Source: Nigerian shape file, NGSA, 2014).

1.4 Statement of Research Problem

Cassiterite are trapped in the topographic lows within drainage basin sinks. Residents around the drainage sink engage in exploration of these Cassiterite deposits. Like in most mining sites in Nigeria, the search for this mineral in Pingel village is done mainly by artisan miners. These miners employ the technique of ‘trial by error’ to search for minerals by indiscriminately digging mining pits (Plate 1.1 A,B). This approach is cumbersome, time-consuming, inaccurate and may even be harmful to miners hence the need for appropriate scientific approach.

One of the major consequences of colonial rule in and around the study area was the influx of immigrants. This rapid increase in population led to the growth of the area, which became both the administrative and commercial Capital of the Province. Cassiterite production attracted huge influx to the area. Most of them came either as voluntary or forced labourers. Cassiterite Mining activities had adverse effects on the people. These resulted in the alienation and destruction of farmlands, diversion of labour from food production, environmental degradation, exploitation of surplus from the peasants and shortage of food.



1.1A

1.1 B

Plate 1.1(A, B): Artisinal Miners Digging and Removing Samples from Mining Pits.

1.5 Justification

According to Pratt *et al.* (1992), the Nigerian Younger Granite is a Petro-geologic supermarket. Cassiterite is one of the most important minerals types of the Nigerian Younger Granite environments. Cassiterite mining is seen to be the major source of employment for residents of the Nigerian younger granite province. Cassiterite is used to prevent rusting or corrosion by simply using it to coat other metals like tin can. It can and equally be used to form many useful alloys such as soft solders, pewter, bronze and phosphor bronze. Circuit-boards for televisions, computers, microwave ovens etc. contain tin because it has a low melting point which makes it ideal for this purpose. If the experiments for electric car use in countries like China and Germany are successful, this could further increase the demand for tin (Akanbiet *al.*, 2012). Thus, the demand for Cassiterite has led to a continuous search for economically viable deposits.

Artisanal cassiterite mining is a major source of employment for people residing in areas within the Nigerian Younger Granite Province. Despite the importance of this means of livelihood artisanal miners do not have any scientific method of detecting areas of high cassiterite potential; hence they resort to trial-and-error methods. The most significant uses of cassiterite are in electronic industries such as circuit-board for television, computers microwave oven etc. Tin-plating which is used as a protective coating on steel cans, for production of bronze and various chemical processes. It is also used in lithium-ion batteries (Cowie, 2010). As a result of the high demand for tin uses worldwide; the federal government has come-up with a policy of developing more mining methods as part of its poverty alleviation programme. Hence, geophysical investigation is needed to ascertain the

probable depth and position of high potential of the cassiterite and columbite reserve of the area.

Although several works concerning Cassiterite mineralization in Nigeria have been documented, to the best of my knowledge, no published data on geophysical work done to suggest the best resistivity configuration for delineation and characterization of Cassiterite mineralization.

1.6 Aim and Objectives of the Study

This research is aimed at using 2D electrical resistivity to characterize the cassiterite (tin ore) bearing layer at MagamaGumau, Bauchi State, Nigeria.

The specific objectives are:

- i. To determine the resistivity electrode configuration that is best suitable for the exploration of the deposit in the study area.
- ii. To generate a 2D resistivity tomography of the study area
- iii. To estimate the range of resistivity values that is associated with the subsurface layer that is rich in the deposit.
- iv. To estimate the depth, thickness, and depth range of the subsurface layer that is rich in the cassiterite deposit.

CHAPTER TWO

LITERATURE REVIEW

2.1 Previous Works on Cassiterite Mineralization and Exploration

Several works have been done on the mineralization of cassiterite in Nigeria. However, on the basis of available literatures, to the best of my knowledge, no published data on geophysical work has been carried out in the study area. This is because it's a newly discovered mining site. A few of the available works are discussed below;

Ikpokonte (1984) carried out gravity and magnetic studies of the sub-basalt cassiterite deposit in plateau state and concluded that the area of investigation includes a possible down-stream extension of the ancient N'gell river basin.

Abubakar *et al.*, (2009) undertook a study of the potential of tailings of Bukurucassiterite deposits for production of iron ore pellets. The study entails the separation and analysis of magnetic minerals mostly iron ore from the tin ore and concluded that the Bukurucassiterite contains sufficiently high-grade iron ore that could be beneficial for iron production.

Akanbiet *al.*, (2012) carried out mapping potential of cassiterite deposit of Naraguta area, Northcentral Nigeria using geophysics and geographical information system, the survey was used to identify cassiterite potential zones in order to contribute towards systemic mineral exploration in the area. They concluded that most of the area within the Jos-Bukuru Complex has high to very high cassiterite mineralization potential.

Abdelwahab (2013) used 2D and 3D resistivity imaging methods to study shallow subsurface structures and compare three conventional resistivity arrays within parts of the University of Baghdad, Iraq. He utilized the dipole-dipole, Wenner-Schlumberger and the

Wenner arrays for his studies and concluded that the Wenner array is the most suitable for 2D and 3D resistivity imaging of the study area.

Ogungbemi *et al.* (2014) used an integrated approach (VLF-EM and electrical resistivity methods) to solid mineral exploration at Kusa Mountain, IjeroEkiti, Southwestern Nigeria. They observed a W-E trending mineralized zone in the area and inferred layers suspected to be mineralized to have resistivity values ranging from 661- 1590 Ωm at thickness between 2.4 m to 7 m.

Umar *et al.*, (2017) undertook geophysical investigation at Rafin-Bareda drainage Basin, Dutsen-Wai, Nigeria using electrical resistivity method in order to identify suitable points of high Cassiterite potential. The result showed that depth to basement rocks, resistivity and thickness values range from 4.5-36.40 m, 59-1,724 Ωm and 1.12-36.40 m respectively. They suggested that areas with high depression on the basement rock represent promising points for Cassiterite deposition.

Akanbiet *et al.*, (2017) used 2D electrical resistivity survey method for mapping of Cassiterite potentials Jos-Bukuru area, Northcentral, Nigeria. The result revealed the probable average depth to cassiterite bearing alluvium to be 6 m.

Al-Hameedawi and Thabit, (2017) used 2D electrical resistivity imaging technique to compare between four electrode arrays in delineating sedimentary layers of alluvial fan deposits in Eastern Iraq. They employed the Dipole–Dipole, Wenner–Schlumberger, Schlumberger reciprocal and Wenner arrays to examine their resolution and ability in delineating the layers in complex sedimentary deposits. The results showed that Wenner–Schlumberger’s inverse models provide optimal results corresponding to the deep

subsurface layers within the area and they also show the best resolution with depth compared to the other arrays.

Ogwuche (2018) conducted magnetic and 2D electrical resistivity survey at Saura village, Keffi, Nasarawa State, Nigeria in order to delineate and characterize pegmatitic structures hosting minerals and gemstones such as Cassiterites, tourmaline, topaz and beryl. His result revealed a NW-SE trend of pegmatitic structures within the area at a depth of approximately 5 m and resistivity between 150 Ωm – 1,000 Ωm to mineral hosting pegmatites.

2.2 Tin Mineralization in Nigeria

Tin minerals, particularly cassiterite are one of the mineral endowments of Nigeria (Okunlola, 2006; 2017). There are two tin provinces in Nigeria. These provinces form parts of the four major metallogenic provinces of the country (Woakes, 1988). The four metallogenic provinces of Nigeria (Figure 2.1) are; Sn-Ta-Nb Pegmatite Belt of Late Pan-African age, Sn-Nb-Ta Younger Granite Province of Jurassic age, Pb-Zn Province of the Benue Trough of Cretaceous age and Au Province of Western Nigeria.

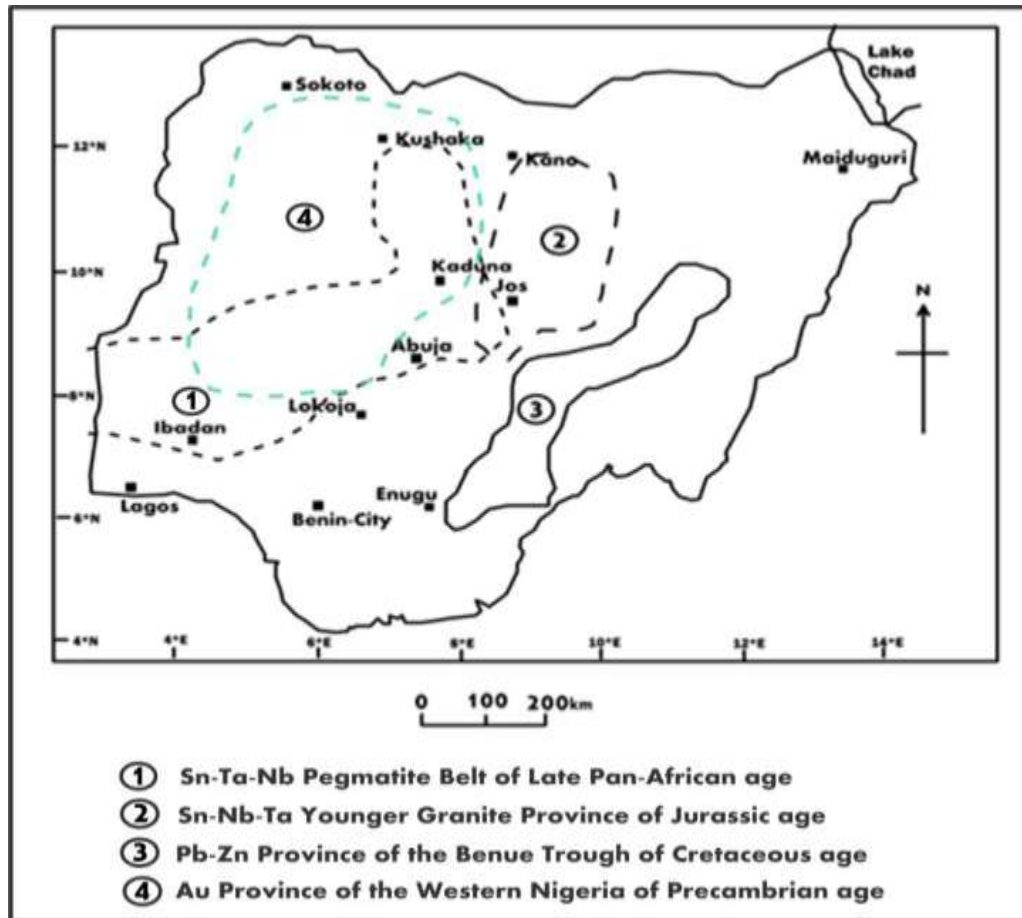


Figure 2.1: Metallogenic Map of Nigeria(modified afterWoakes, 1988; Garba, 2003).

2.2.1 Sn-Ta-Nb Pegmatite Belt of Late Pan-African age

The Sn-Ta-Nb Pegmatite Belt of Nigeria consist of over 3,000 tin-bearing pegmatites of diverse mineralogy, structural orientations and chemical compositions ranging between 10m – 1,500 m in length and sometimes up to 50 m in width occurring in granites, schists, gneisses, amphibolites and quartzites (Okunlola, 2006; 2005). The mineralized pegmatite belt extends from southwestern (Ijebu area) to northern Nigeria (through Wamba-Jema’a to Zuru-Gusau area) covering a broad, over 400km long zone trending NE–SW and parallel to the linear pattern of the other two metallogenic provinces (Younger Granite and Cretaceous Benue Trough provinces) (Okunlola, 2006; 2005; 2008; Matheis&Emofurieta, 1990). The

pegmatite belt of Nigeria is presumed to extend into northeast Brazil (Garba, 2003; Morteau *et al.*, 2000; Beurlenet *et al.*, 2008). The mineralized or rare metal-bearing pegmatites consist mainly of quartz, potash feldspar, albite, muscovite and less commonly, biotite and a range of accessory minerals including tourmaline, beryl, aquamarine, lepidolite and economically important cassiterite, columbite and tantalite.

The mineralized pegmatite belt, also known as the Older Tin field of Nigeria, is the only basement metallogenic feature that cross-cuts the schist belt structures although most pegmatites are oriented N-S (Matheis & Emofurieta, 1990; Wright, 1970). The belt is divided into 3 zones: (i) the main central Nigerian pegmatite belt (ii) area of richest stanniferous pegmatites (iii) and area of subordinate mineralization (Figure 2.2).

Notable mineralized pegmatites are found in Ijero, Sepeteri, Aramoko, Ife-Ilesha, Ikoro, Osu, Igbeti, Oro, Oke-Ogun, Komu, Egbe, Akata, Wamba-Jema'a, Keffi, Akwanga, GwonGwon, and Jos Plateau, all occurring within the Nigerian mineralized pegmatite belt. A few occurrences of poor – low grade tin-bearing pegmatites have also been found outside the pegmatite belt in the Obudu and Oban massifs in southeastern Nigeria (Okunlola, 2005; 2008; Ero & Ekwueme 2009; Ministry of mine and steel, 2012). The mineralized pegmatites have yielded about 5% of the total cassiterite produced in Nigeria (Okunlola, 2006; Matheis, 1979).

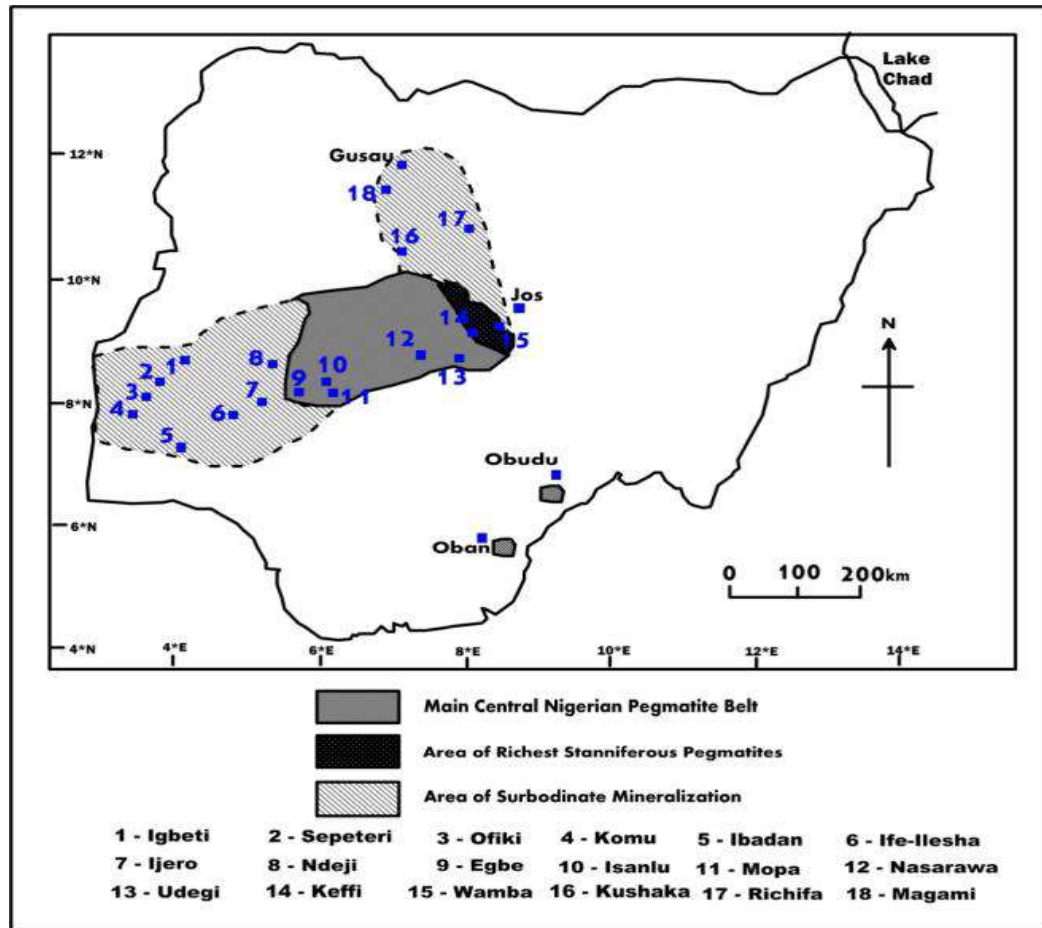


Figure 2.2: Map showing the locations of notable tin-bearing pegmatites in Nigeria (Garba, 2003; Okunlola, 2005; Wright, 1970).

The Nigerian tin-bearing pegmatites are probably related to the Pan-African Older Granite suite which often occurs in close proximity. The mineralized pegmatites were formed due to magmatic differentiation processes during late Pan-African orogenic event, in the range 580 – 500 Ma (Matheis, 1987). They are younger than the Older Granites and barren pegmatites but older than the Younger Granites. Tin-bearing pegmatites associated with metasedimentary rocks (schists, paragneisses and quartzites) in schist belts (as in Ijero, Egbe, Ilesha) suggest metamorphic or metasomatic replacement processes (particularly late-stage albitization) are important in their formation (Obaje, 2009; Wright, 1970).

2.2.2 Sn-Nb-Ta Younger Granite Province of Jurassic Age

The Younger Granite Province in north central Nigeria, trending NE-SW, covers a total area of about 7,500 km². The province consists of over 50 massifs of anorogenic complexes (Figure 5) made up of both volcanic (rhyolites, trachyte and basalts) and plutonic rocks (aegirine-, arfvedsonite-, riebeckite-, biotite- and hornblende-bearing granites, syenites, quartz porphyry, granite porphyry and gabbro) formed during the Mesozoic, probably related to the early break-up of Gondwanaland and splitting of Africa from South America. This event was also responsible for the opening up of the Benue Trough (Wright, 1981). The Younger Granite Province terminates the Sn-Ta-Nb Pegmatite belt in the east. Wright (1970), referred to the Younger Granite Tin Province as Younger Tin field of Nigeria.

Tin ores (cassiterite and stannite) occurs in the Younger Granite complexes in two primary forms: (i) disseminations and (ii) veins and greisens. Disseminations of accessory cassiterite occur in association with columbite, tantalite and other ores (monazite, zircon, cryolite, rutile, ilmenite, genthelvite, beryl, molybdenite, sphalerite and chalcopyrite) in the roof zones and margins of peraluminous biotite granites in most of the Younger Granite Complexes, but known enrichment is focused in parts of the Jos-Bukuru, Tongolo, Tibchi, Dutsen-Wai and Afu complexes.

The peralkaline granites, inspite of their high Sn content as revealed by chemical analyses, contain no cassiterite ore. This suggests that Sn did not occur as cassiterite but probably remains dispersed in the sodic-bearing minerals (Olade, 1980; Imeokparia, 2015). However, the peralkaline albite-riebeckite granites contain significantly high concentrations of niobium, zinc, uranium and zirconium (Ogunleye *et al.*, 2004).

Few highly mineralized quartz-sulphide-cassiterite veins and greisens enriched in cassiterite, stannite, sphalerite, galena, columbite, chalcopyrite, siderite, arsenopyrite, wolframite and bismuth minerals occur within fractures and along the margins of Younger Granite rocks. These are the most economically viable primary tin deposits in the province. Notable cassiterite-bearing veins or lodes and/or greisens occur in the Ririwai, Tibchi, Tongolo and Afu complexes (in decreasing order of mineralisation).

Over 95% of the tin (cassiterite) produced in Nigeria was mined in the Younger Granite Province and were won from alluvial deposits derived from the tin-bearing granites and lodes. The origin of the Sn-Nb-Ta mineralization in the Younger Granite Province is related to the petrogenesis of the Younger Granites. Wright (1970), suggested that cassiterite and its associated ore minerals in the Younger Granite ring complexes of Nigeria were not basement-derived, but originated at deeper levels as part of the primary melts. This suggestion was based on the premise that the Younger Granite magmas probably originated in the upper mantle, as salic melts, generated by pressure relief, partial melting, and a concentration of low melting constituents beneath a broad crustal dome, and modified by interaction with basement rocks (Kinnaird *et al.*, 2016).

2.2.3 The History of Tin Mining in Nigeria 1904 – 1960.

One of the ways by which man impacts on his environment is through mining activities. Tin mining industry is one of the oldest industries in the world and its importance cannot be over emphasized. Mining on the whole is the extraction of valuable mineral resources or other geological minerals from the earth, usually from an orebody, vein or seam. It can also be said to be an act or process of extracting minerals of economic importance from their natural environment and transporting them to points of processing and use.

Mining in Nigeria started as far back as in the eighteenth century. Over 500 occurrences and deposits of different minerals are known far to exist within the country with the exploration of some being on a smallscale (Adegbulugbe, 2010). One of the major cases of mineral exploration and exploitation that boomed within the nation has been that of Tin ore in Jos-Plateau. Tin is said to be one of the oldest mineral resources known to man as its valuable importance was recognized or noticed as far as some 300 years ago when its hardening effects on copper was discovered (Adegbulugbe, 2010). Since then, tin ore have been mined in several parts of Nigeria including Zaria, Kano, Bauchi, Ilesha and Plateau Province, with over 80% of the production coming from the Jos Plateau (Ajaegbu, 1992).

The tin mining industry in Jos Plateau started in 1904 during the colonial era. After the survey of the area in 1902, the expatriate mining of tin ore began in 1904 despite the resistance offered by the people. From then onwards, the British extracted large quantities of tin ore from the Jos Plateau such that by 1938 Nigeria's export of tin ore to Britain stood at 10,486 tons which was valued at £1,435,157. It rose to 11,164 tons in 1951-52 and 11,942 tons in 1952-53 (Adegbulugbe, 2010).

Many people got attracted to Jos Plateau as a result of tin mining, while a few to Naraguta and Delimi where mining activities also took place. During this period, only very few people worked in government establishments as labourers and messengers. Those who worked in the mining camps were immigrant Hausa people or Kanuri from Kano, Zaria, Bauchi and as far as the Emirate of Bornu and Chad Region (Adegbulugbe, 2010).

Very few local people were attracted to the mining settlement at the initial stage. Economic importance and wealth were then recorded not by the amount of money a person had, but on how much crops, animals, wives et cetera, a person had. For this reason, the expansion of

farmland was more attractive to the hill farmers at this period than going to work in the mines and to live in mining camps.

Again, it can be added that tradition permeated nearly all their lives. It was therefore difficult to bring about any change in their economic activities especially as their customs, religious beliefs and ceremonies were all closely bound up with the land and not mining on a large scale.²⁰ Monetary advantage was thus not necessarily the aim of the hill-tribes, hence the majority of the people of the Naraguta village and mining camp were Hausa. This is the reason why the term Hausa Town was applied to their residential quarters up to 1913.

Besides the miners and other workers, the settlement attracted itinerant traders from Bauchi, Zaria and Kano. However, by 1913 the miners came to discover that the richest deposits of tin ore lay not around Naraguta but to the South of it and most of the mining activity was taking place near the upper reaches of Delimi Rivers around Gangare, Ray field and Bukuru. This led to the establishment of Gangare as the largest mining camp along the Delimi River. This further attracted miners from their original settlement to Gangare which in fact is in the east of Jos town today.

Some of the industries involved in mining at that time were British Tin Mining Corporation, Bisichi-Jenta, Gold and Base, Exland and Kaduna Prospectors. The Tin Mining Industry suffered severely during the economic depression of the 1930s and so did Jos and its population. It was recorded that 47 out of 122 mining concerns were closed down by 1933. According to Plotnicov, most of the residents of Jos at this period were southerners. He associated this with large number of southerners and non-Nigerians who were traders or skilled workers in the mines and the railways or commercial firms. Their skills according to him were scarce at the time and their employers had to retain them

so that the retrenchment which followed the depression of the 1930s, did not affect many of them. This may be true but it is difficult to agree with Plotnicov here because there is no evidence to prove that there were more Southerners than other Northern tribes in Jos at this period. However, a significant proportion of the town's commercial activities at this period was in the hands of Southern Nigerians and oriented towards the needs of the mining industry. By the late 1950s when Tin Mining activity in the Jos Plateau started experiencing a lull, the aforementioned industries metamorphosed into what is now known as consolidated Tin Mining of Nigeria Limited. But unfortunately, after the departure of the former, the government failed to finance remediation efforts to the mining industry.

2.3 Principle of the Electrical Resistivity Method

In the resistivity methods, artificially generated electric current are driven into the ground. Any variation in subsurface resistivity (conductivity) alters the current flow patterns which in turn affect the distribution of electric potential. The resulting potential differences established are measured at the surface. Any variations observed from the pattern of potential differences expected from uniform earth are deviations from the uniform earth. These deviations represent the geological target of resistivity exploration.

Placing two electrodes in the ground at a distance from each other and sending current between them causes an electrical field to spread into the earth around them. The potential of the field decreases with distance from the electrodes and is always at its maximum on a line between them (figure 2.3). The electrical field penetrates more deeply into the subsurface when the current electrodes are farthest from each other, rather than when they are relatively close together. By measuring the difference in potentials (M and N) between two electrodes within that induced field, the resistance of the earth can be

measured. Multiplying the resistance by a geometric constant derived from the relative positions of the current and potential electrodes, yields the resistivity of the material beneath the electrodes.

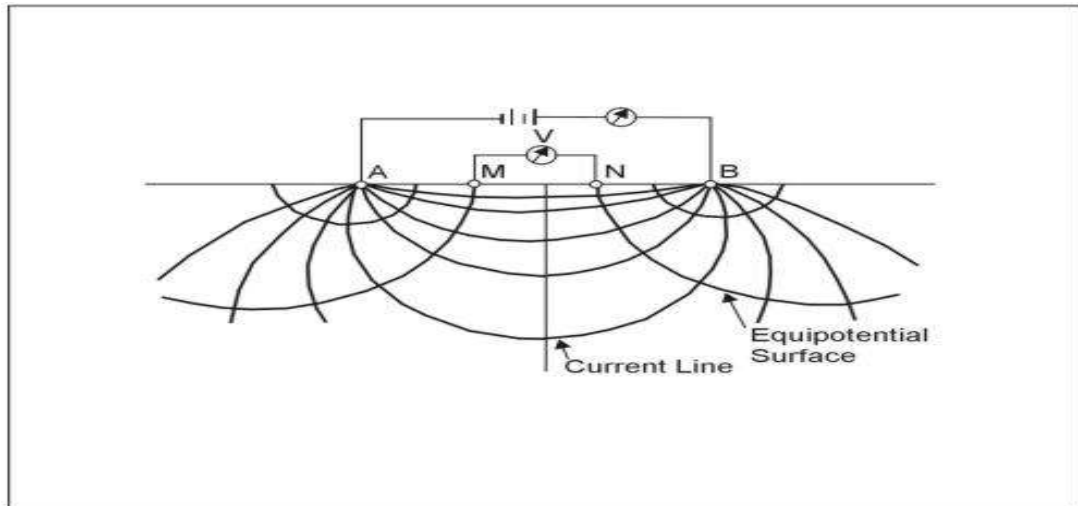


Figure 2.3: Current flow lines and equipotential between two current electrodes A and B.

The advent of automated multi-electrode resistivity systems has led to rapid and efficient data acquisition of resistivity measurements. Using a number of electrodes attached to a resistivity system with a switching module makes it possible to carry out 2D, 3D and 4D imaging surveys with tremendously increased efficiency and productivity. Multi-electrode resistivity systems, however, are based on using the principle of a four-electrode method and the adoption of multiplexing of a number of electrodes. A computer-controlled switching module chooses four predefined electrodes for each single measurement, sends the current, and measures the potential drop from which the resistance can be calculated (Loke *et al.*, 2011). Using a number of various combinations of transmitting and receiving pairs of electrodes, 2D/3D resistivity images can be constructed using appropriate inversion software. Moreover, using time-lapse 3D resistivity technique, 4D resistivity data can be

obtained (Chambers *et al.*, 2013). These improvements provide much more detailed information than the traditional 1D resistivity sounding, profiling and mapping.

Resistivity data, however, can be obtained using different array arrangements. An example of 2D data collection using 20 electrodes with a Wenner array (Loke *et al.*, 2013), is shown in figure 2.4.

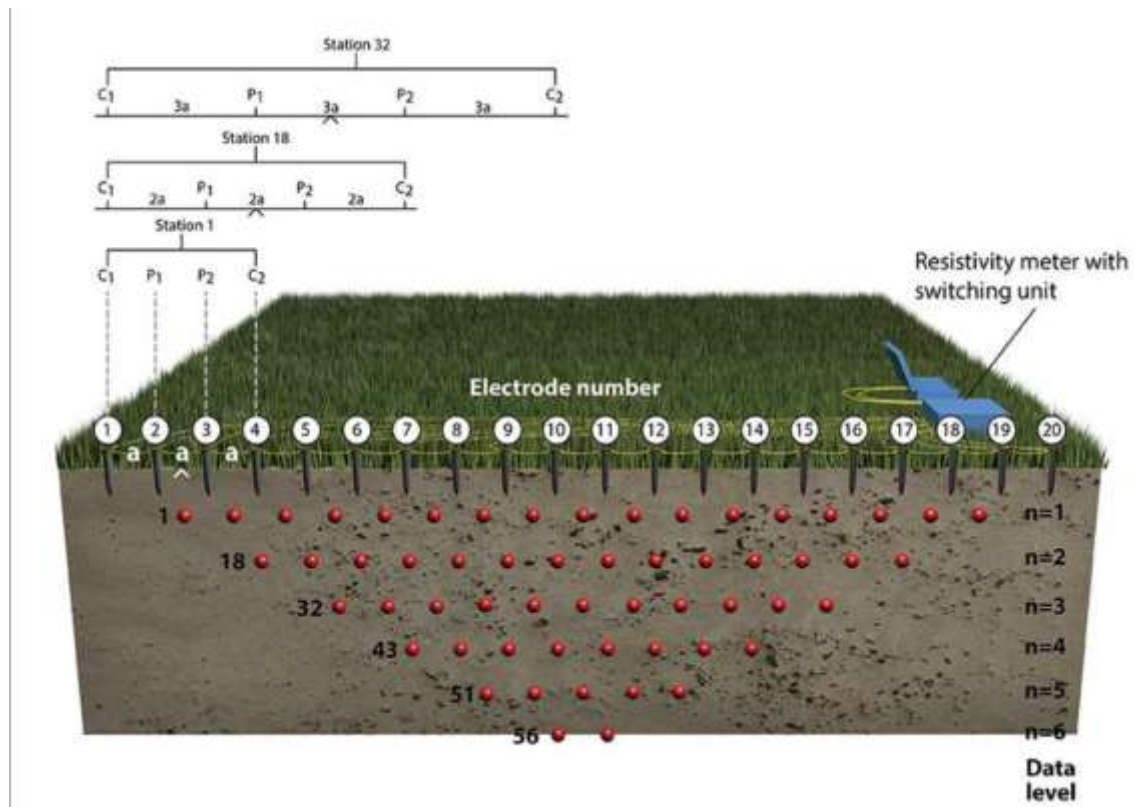


Figure 2.4: 2D data collection using multi-electrode resistivity system (Loke *et al.*, 2013).

Resistivity survey determine the variation in the- electrical resistivity of the subsurface by applying electric current across arrays of surface electrodes (Loke, 1999). From this measurement obtained, the true resistivity of the subsurface can be estimated. This development started with the introduction of practical electrical tomography field systems, like the geoelectrical Wenner pseudo section and was soon followed by effective

processing and inversion software. The ground resistivity is related to various geological parameters such as the mineral and fluid content, porosity and degree of water saturation in the rock.

The classical methods of resistivity survey have undergone significant changes in the last three decades. The traditional horizontal layering technique for interpreting geoelectrical resistivity data are rapidly being replaced with two-dimensional (2D) and three-dimensional (3D) models of interpretations, especially in complex and heterogeneous subsurface media. Field techniques have advanced from measurements made at separate and independent points to automated measuring systems with multi-electrode array along the measurement profiles. Data acquisition was more or less carried out manually until the 1980s, and this is labour intensive and slow and the quality of measured data might be poor. A range of fast automated multi-electrode and multi-channel data acquisition systems now exist that allow flexibility in the acquisition of geoelectrical resistivity data (Barker, 1981; Stummer and Maurer, 2001; Auken *et al.*, 2006, Aizebeokhai, 2010).

2.3.1 Theory of the Resistivity Method

The principle underlying the resistivity method is embodied in Ohm's law, which states that the electrical current flowing in a circuit is proportional to the voltage and inversely proportional to the resistance. Thus, Ohm's law gives the relationship between current density J (amperes/m²) and electric field intensity E (volts/m) as:

$$J = \sigma E \quad (2.1)$$

Where σ is the conductivity of the medium. Also, E is the gradient of a scalar potential U (volts), i.e.

$$E = -\nabla U \quad (2.2)$$

Putting equation (2.2) into equation (2.1)

$$J = -\sigma \nabla U \quad (2.3)$$

From divergence condition,

$$\nabla \cdot J = 0 \quad (2.4)$$

Thus, from equation (2.3)

$$\nabla \cdot J = -\nabla \cdot (\sigma \nabla U) = 0 \quad (2.5)$$

Or,

$$\nabla \sigma \cdot \sigma U + \sigma \nabla^2 U = 0 \quad (2.6)$$

For a homogeneous earth, σ is a constant and since the derivative of a constant is equal to zero, then the first term in equation (2.6) vanishes hence,

$$\nabla^2 U = 0 \quad (2.7)$$

Equation (2.7) is called Laplace equation.

Applying boundary conditions, equation (2.7) can be solved for specific cases. For instance, for a single current electrode at the surface of a homogeneous ground, equation (2.7) is expressed in spherical polar coordinates as:

$$\frac{1}{r} \frac{\partial}{\partial r} \left(r^2 \frac{\partial U}{\partial r} \right) + \frac{1}{r^2 \sin \theta} \frac{\partial}{\partial \theta} \left(\sin \theta \frac{\partial U}{\partial \theta} \right) + \frac{1}{r^2 \sin^2 \theta} \left(\frac{\partial^2 U}{\partial \phi^2} \right) = 0 \quad (2.8)$$

For point current source, there is complete symmetry of current flow with respect to the θ and ϕ directions and the derivatives with respect to these directions are zero. Thus, equation (2.8) becomes;

$$\frac{\partial}{\partial r} \left(r^2 \frac{\partial U}{\partial r} \right) = 0 \quad (2.9)$$

Integrating the equation twice gives;

$$r^2 \frac{dU}{dr} = a \quad \text{and} \quad U = -\frac{a}{r} + b$$

where **a** and **b** are constants, U is the electric potential at the measuring point and r is the distance from that point to the single current electrode. Since $U = 0$ as $r \rightarrow \infty$ then $b = 0$ and

$$U = -\frac{a}{r} \quad (2.10)$$

The current flows radially outwards in all directions from the point current electrode and the total current crossing a sphere of radius **r** is;

$$I = 4\pi r^2 J = -4\pi r^2 \sigma \frac{dU}{dr} = -4\pi \sigma a = -\frac{4\pi a}{\rho} \quad (2.11)$$

After using equation (2.3) and equation (2.10). Thus,

$$a = -\frac{I\rho}{4\pi} \quad (2.12)$$

Substituting equation (2.12) into equation (2.10) we have;

$$U = \frac{I\rho}{4\pi} \frac{1}{r} \quad \text{Or} \quad \rho = 4\pi r \left(\frac{U}{I} \right) \quad (2.13)$$

The equipotential which are everywhere perpendicular to the current flow lines will be spherical surfaces given by r is equal to a constant.

The point current electrode of the three-point-system is located at the surface of the homogeneous isotropic medium θ the air above having zero conductivity, the return current electrode is at a great distance. As in the previous case $b=0$ since $U=0$ as $r \rightarrow \infty$

In addition, $\frac{\partial U}{\partial z} = 0$ at $Z = 0$

Since $\sigma_{air} = 0$ In the present case, all the current flows through a hemispherical surface in the lower region.

Hence,

$$\alpha = -\frac{I\rho}{2\pi} \quad \text{and} \quad U = \frac{I\rho}{2\pi r} \quad \text{or} \quad \rho = 2\pi r \left(\frac{U}{I}\right) \quad (2.14)$$

When the distance between two current electrodes is finite (figure 2.5), the potential at any nearby surface point will be affected by both current electrodes. As seen from equation 2.14, the potential due to C_1 at P_1 is:

$$U_1 = -\frac{A_1}{r_1} \quad \text{where } A_1 = -\frac{I\rho}{2\pi} \quad (2.15)$$

Because the currents at the two electrodes are equal and opposite in direction, the potential due to C_2 at P_1 is:

$$U_2 = -\frac{A_2}{r_2} \quad \text{Where } A_2 = \frac{I\rho}{2\pi} = -A_1 \quad (2.16)$$

Thus, we can have;

$$U_1 + U_2 = \frac{I\rho}{2\pi} \left(\frac{1}{r_1} - \frac{1}{r_2} \right) \quad (2.17)$$

Finally, by introducing a second potential electrode at P_2 , we can measure the difference in potential between P_1 and P_2 which will be:

$$\Delta U = \frac{I\rho}{2\pi} \left\{ \left(\frac{1}{r_1} - \frac{1}{r_2} \right) - \left(\frac{1}{r_3} - \frac{1}{r_4} \right) \right\}$$

$$\Delta U = \frac{I\rho}{2\pi} \left[\frac{1}{r_1} - \frac{1}{r_2} - \frac{1}{r_3} + \frac{1}{r_4} \right] \quad (2.18)$$

Such an arrangement corresponds to the four-electrode spread normally used in resistivity field work, where ρ is the resistivity, I is the current and r_1 , r_2 , r_3 , and r_4 , are the inter-electrode distances.

From equation 2.18, the apparent resistivity can be solved for as;

$$\rho_a = \frac{\Delta U}{I} \frac{2\pi}{\left[\frac{1}{r_1} - \frac{1}{r_2} - \frac{1}{r_3} + \frac{1}{r_4} \right]} \quad (2.19)$$

The result is independent of the position of the electrodes and is not affected when the current and the potential electrodes are interchanged.

The resistance is calculated using Ohm's law:

$$R = \frac{\Delta U}{I} \quad (2.20)$$

Where, R is the resistance in ohms; ΔU is the potential difference in volts; and I is the current in amperes.

The material parameter ρ which is the inverse of electrical conductivity σ is related to the resistance via a geometric factor K' that is a function of the electrode configuration. The resistivity of the homogeneous ground can be calculated using, the relation;

$$\rho = K' \frac{\Delta U}{I} \quad (2.21)$$

Where;

$$K' = \frac{2\pi}{\left[\frac{1}{r_2} - \frac{1}{r_3} - \frac{1}{r_3} + \frac{1}{r_4} \right]}$$

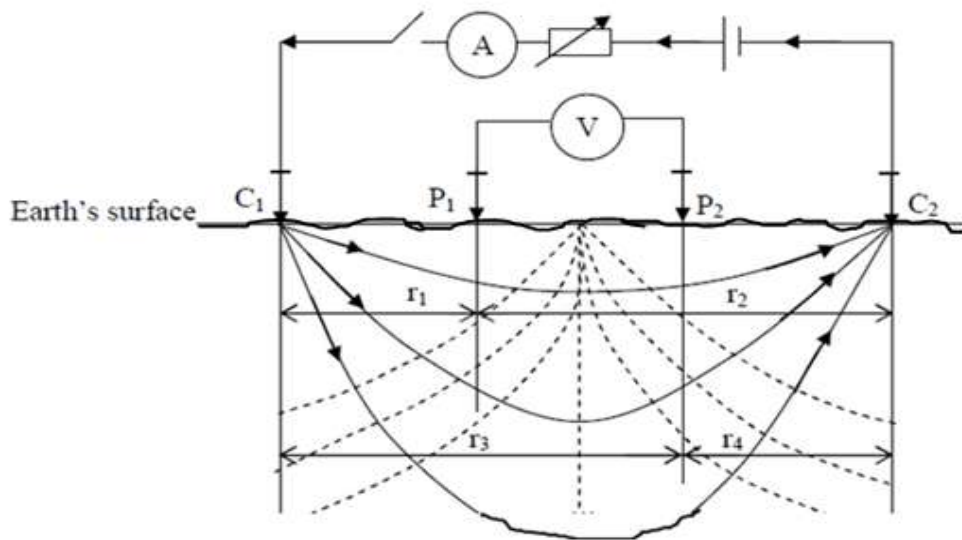


Figure 2.5: General-four electrode arrangement.

2.4 Electrical Resistivity Configurations

Electrode configurations or arrays are different arrangements of electrodes used to perform geophysical resistivity measurements. They were developed in order to make field measurements more efficient and data interpretation easier. Several number of electrode spreads have been used in resistivity at various times however only a few have survived to any extent (Telford *et al.*, 1990). One drawback in resistivity work is the practical difficulty of moving stakes with great lengths of wire attached, a slow and expensive task in relation to other geophysical methods. Thus, it is an advantage to use electrode spreads with less cumbersome field procedure. Of all the electrical resistivity configurations, the Wenner, Schlumberger and the dipole-dipole (double dipole in some literatures) are the most widely used configuration largely due to the relative ease in their field procedure.

2.4.1 Wenner Configuration

The Wenner array (Figure 2.6) was invented in 1915 by American physicist Frank Wenner (1873-1954). His development of a four-terminal bridge design consisting of two outer current injection electrodes and two inner potential electrodes equally spaced became known as the “Wenner array.” It is the simplest of arrays in that the four electrodes are placed in line and spaced equidistant from each other. The two outer electrodes, A and B, are current electrodes, and the two inner electrodes, M and N, are potential electrodes. The Wenner array is commonly used in profiling for lateral exploration of the ground, like soil testing and sometimes VES for vertical exploration of the ground, like defining horizontal layers. The logistic advantage of using the Wenner array when profiling is that one only has to move four electrodes for each new measurement along the line.

In general, the Wenner is good in resolving vertical changes (i.e. horizontal structures), but relatively poor in detecting horizontal changes (i.e. narrow vertical structures). Compared to other arrays, the Wenner array has a moderate depth of investigation. The signal strength is inversely proportional to the geometric factor used to calculate the apparent resistivity value for the array. Hence, among the common arrays, the Wenner array has the strongest signal strength. This can be an important factor if the survey is carried in areas with high background noise. One disadvantage of this array for 2-D surveys is the relatively poor horizontal coverage as the electrode spacing is increased. This could be a problem if you use a system with a relatively small number of electrodes.

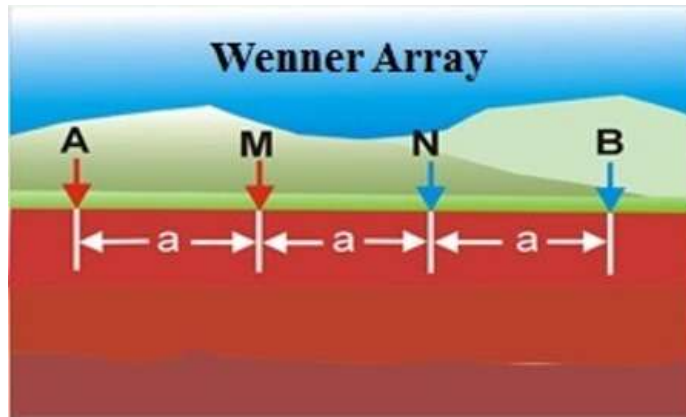


Figure 2.6: The Wenner Configuration (Balogun, 2017)

2.4.2 Schlumberger Configuration

The Schlumberger array is named for Conrad Schlumberger, founder of the modern-day Schlumberger oilfield Services Company and pioneer of electrical methods in the early 1900s.

The Schlumberger array (Figure 2.7) is an array where four electrodes are placed in line around a common midpoint. The two outer electrodes, A and B, are current electrodes, and the two inner electrodes, M and N, are potential electrodes placed close together. With the Schlumberger array, for each measurement the current electrodes A and B are moved outward to a greater separation throughout the survey, while the potential electrodes M and N stay in the same position until the observed voltage becomes too small to measure. At this point, the potential electrodes M and N are moved outward to a new spacing. As a rule of the thumb, the reasonable distance between M and N should be equal or less than one-fifth of the distance between A and B at the beginning. This ratio goes about up to one-tenth or one-fifteenth depending on the signal strength.

The Schlumberger array is commonly used for vertical electrical sounding (VES) for groundwater and aggregate minerals. VES using the Schlumberger array provides better resolution, and take less time to deploy than the other arrays.

The Schlumberger array is the best method for VES for practical reasons—it is significantly less labor-intensive than the Wenner array. For VES in general, the Schlumberger array is at advantage, because most of the time only the outer electrodes A and B need to be moved. A crew of three people is normally enough for VES—with two people moving the outer electrodes, the instrument operator typically moves the inner electrodes the few times they need to be moved.

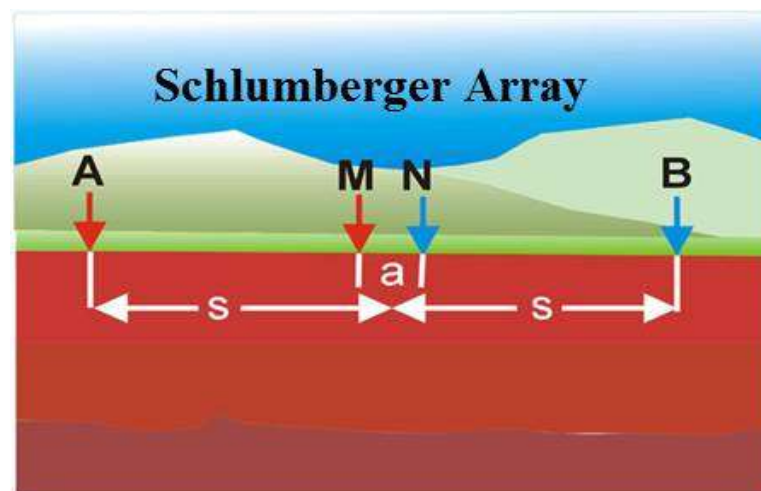


Figure 2.7: The Schlumberger Configuration (Balogun, 2017).

2.4.3 Dipole-Dipole Configuration

This array has been, and is still, widely used in resistivity and IP surveys because of the low EM coupling between the current and potential circuits. The arrangement of the electrodes is shown in figure 2.8. The spacing between the current electrodes pair, A-B, is given as “a” which is the same as the distance between the potential electrodes pair M-N. This array has another factor marked as “n”. This is the ratio of the distance between the A and M electrodes to the A-B (or M-N) dipole length “a”. For surveys with this array, the “a” spacing is initially kept fixed at the smallest unit electrode spacing and the “n” factor is increased from 1 to 2 to 3 until up to about 6 in order to increase the depth of investigation. The dipole-dipole array is the most sensitive to resistivity variations below the electrodes in each dipole pair and is very sensitive to horizontal variations but relatively insensitive to vertical variations in the subsurface resistivities (Okpoli, 2013). Thus, it is the most preferred array for mapping vertical structures like dykes and cavities. Additionally, it is the most sensitive array to 3D structure among the common arrays (Dahlin and Loke, 1997). The depth of investigation of the array depends on both the current electrode spacing and the distance between the two dipoles and is generally shallower than that of Wenner array. However, dipole-dipole array has better horizontal data coverage than Wenner array. The major disadvantage of this array is the decrease in signal strength with increasing distance between the dipole pair.

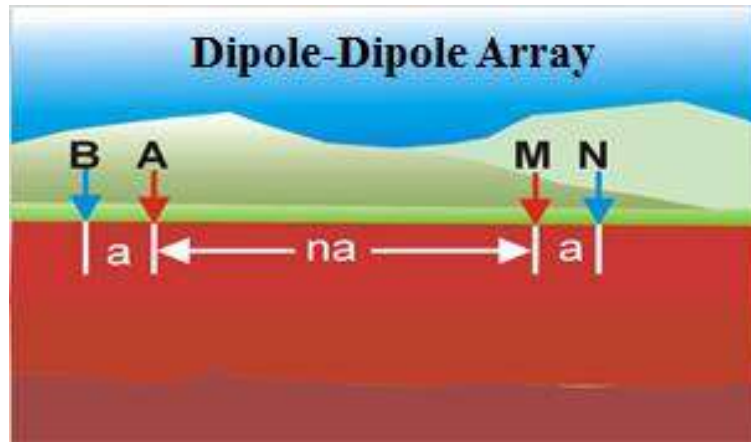


Figure 2.8: The Dipole-Dipole Configuration (Balogun, 2017).

2.5 Resistivity of Rocks, soil and Minerals.

The electrical resistivity of rocks and minerals is an extremely variable property and depends on several factors. Of all the physical properties of earth materials (rocks and minerals), electrical resistivity has the widest range of variation. Resistivity of metallic minerals may be as small as $10^{-5}\Omega\text{m}$ while that of dry close-grained rocks like gabbro could be as large as $10^7\Omega\text{m}$. The maximum possible range is even greater, from native silver, $1.6 \times 10^{-8}\Omega\text{m}$ to pure Sulphur $10^{16}\Omega\text{m}$ (Telford *et al.*, 1990). The common minerals forming rocks and soils have very high resistivity values in dry condition and the resistivity of rocks and soils is therefore normally a function of the amount and quantity of water in pores and fractures. The degree of connection between cavities is also important; consequently, the resistivity of a rock type or soil type may vary widely. The electrical resistivity varies between different geological materials depending mainly on variations in water content and dissolved ions in the water and also texture and grain size. Resistivity investigations can thus be used to identify zones with different electrical properties, which can then be referred to different geological strata. However, the variation may be limited within

confined geological area and variations in resistivity within certain soil or rock type will reflect variations in physical properties. For example the lowest resistivities encountered for sandstones and limestone means that the pore spaces in the rock are saturated with water, whereas the highest values represent strongly consolidated sedimentary rock or dry rock above the groundwater surface. Sand, gravel and sedimentary rocks may also have very low resistivities provided the pores in the rocks are saturated with saline water. Fresh crystalline rock is highly resistive apart from certain ore minerals, but weathering commonly produces highly conductive clay rich saprolite. The variation in characteristics within one type of geological material makes it necessary to calibrate resistivity data against geologic documentation for instance, surface mapping, test pits or drilling. Typical ranges of resistivities of geologic materials are shown in figure 2.9.

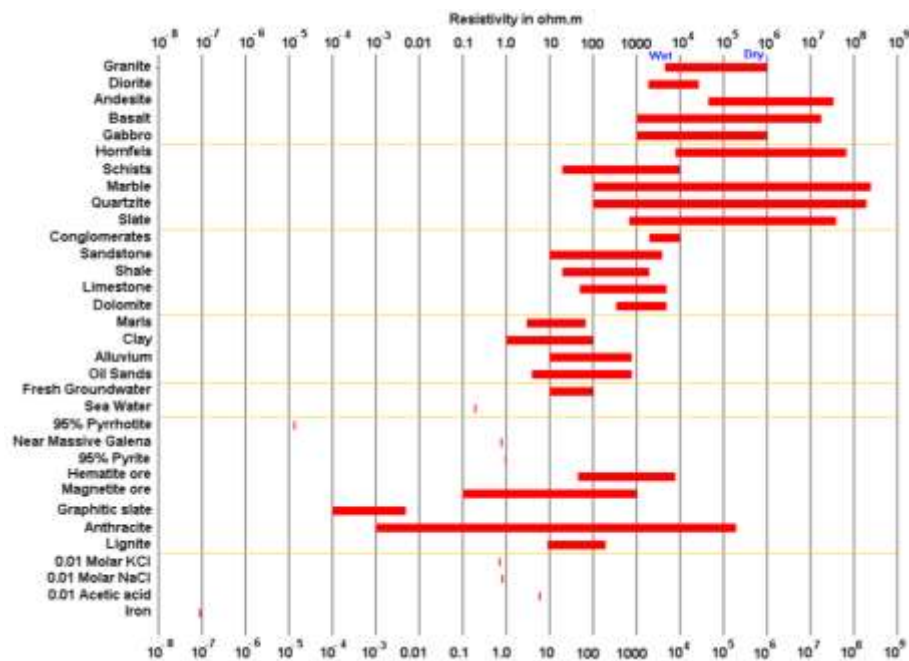


Figure 2.9: Resistivity's of Rocks, Soils and Minerals (Loke, 2010).

2.6 Factors Affecting Electrical Resistivity

The electrical resistivity of rocks and minerals is an extremely variable property and depends on a number of factors. Bulk resistivities from the surface to more than 15 km depth in a normal crust are controlled by aqueous electrolytic conduction by way of pores, fractures, faults, and shear zones. The resistivity of crystalline rock formations such as granulites, granite, and diorite in situ is largely dependent upon the water in the fissures and fractures. Similarly, the porosity, degree of saturation and the nature of pore-electrolytes govern the resistivity of rocks like sandstone and limestone. A slight increase in resistivity with depth is the result of decreasing pore, fracture, fault and shear-zone porosity due to increased lithostatic load.

2.6.1 Water Salinity

Conduction in near-surface rocks is largely electrolytic, taking place in connected pore spaces, along grain boundaries, in fractures, faults and shear zones but negligibly through the silicate framework. The ions which conduct the current result from the dissociation of salts, such dissociation occurring when salts are dissolved in water. Since each ion is able to carry only a definite quantity of charge, it follows that the more ions that are available in a solution the greater will be the charge that can be carried. Hence, the solution with the larger number of ions will have the higher conductivity. In general, for a given porosity, a rock which contains saline water within its pores will have a greater conductivity when the salinity of the water is high than when it is low. Resistivity decreases with increase in salinity.

2.6.2 Porosity of Rock

Porosity can be defined as the ratio of the percentage of the volume of void space to the total volume of the rock. Porosity arises from the fact that the particles do not occupy all the possible space. It provides a direct measure of the total void space available for the storage of fluids.

Resistivity and porosity in sedimentary rocks can be related by the general form of Archie's law, which for rocks devoid of clay is written as

$$F = \frac{\rho_r}{\rho_s} = a\phi^{-m}$$

Where F is the formation resistivity factor, ρ_r is the resistivity of the rock, ρ_s is the resistivity of the solution in the pores of the rock, ϕ is porosity, while "a" and "m" are constants peculiar to the rock type. The constant "m" is usually referred to as the cementation factor while the constant "a" is referred to as the coefficient of saturation.

The most common minerals forming soils and rocks have very high resistivity in a dry condition, and the resistivity of soils and rocks is therefore normally a function of the amount and quality of water in pore spaces and fractures. The degree of connection between the cavities is also important.

2.6.3 Effect of Temperature

An increase in temperature lowers the viscosity of water, with the result that ions in the water become more mobile. The increased mobility of the ions results in an observed resistivity decrease with increase in temperature according to the formula (Keller and Frischknecht, 1966):

$$\rho_t = \frac{\rho_{18^\circ}}{1 + \alpha_t (t - 18^\circ)}$$

Where ρ_{18° is the resistivity measured at a reference temperature of 18°C, α is the temperature coefficient of resistivity (about 0.025 per degree centigrade for most electrolytes) and t is the ambient temperature.

2.6.4 Effects of Rock Texture and Porosity

The texture of a rock dictates its resistivity in the following ways:

- (i) A well-sorted sandstone has large void spaces and hence exhibits low resistivity.
- (ii) A poorly-sorted sandstone will have a much lower porosity and hence will exhibit higher resistivity.
- (iii) Dissolution along fractures in a limestone will enhance porosity and hence lower resistivity.
- (iv) Precipitation of some minerals in any rock will lower the porosity and hence increase resistivity.
- (v) Basalt has much unconnected or dead-end pore space and hence low permeability, so that even basalt of high porosity may exhibit high resistivity.

2.6.5 Effects of Geological Processes

In general, geological processes reduce the resistivity of a rock but there are exceptions.

Weathering or hydrothermal alteration of a granite significantly lowers its resistivity. Dissolution, faulting and shearing usually increase porosity and fluid permeability, and hence lower resistivity. Precipitation of calcium carbonate and silica reduces porosity and hence reduces fluid permeability and increases resistivity. Induration by compaction or metamorphism will reduce porosity and permeability and hence increase resistivity. Salt water intrusion provides more ions for conduction and therefore reduces resistivity.

CHAPTER THREE

MATERIALS AND METHOD

3.1 Instrumentation

In resistivity measurement nowadays, there are a range of instrumentation from very simple to highly sophisticated equipment with the latter including the computer for infield data processing. The basic parts of any resistivity instrumentation are a portable power source which is either a D.C. or a low frequency A.C., Electrodes, preferably stainless-steel electrodes and cable and reels, Global Positioning System (G.P.S.), meters for measuring current and voltage both of which may be combined in a single meter reading resistance or apparent resistivity. With the development of computer-controlled data collection and automatic data inversion, the use of computer-controlled multi-electrode systems with automatic measurement for the data acquisition became very relevant. This is because it gives a dramatic increase in field productivity. Such is the ABEM LUND Imaging System.

3.1.2 ABEM LUNG Imaging System (SAS 1000)

The LUND Imaging System is a multi-electrode system for cost effective and high resolution 2D and 3D resistivity surveys. It is an automatic electric imaging system suited for automatic resistivity profiling and drilling. The LUND Resistivity imaging System consists of a basic unit, a standard resistivity meter (ABEM Terrameter SAS 1000) and a (4x64) multi-channel relay matrix switch unit called Electrode Selector (ES) 464. The system also has four multi-conductor electrode cables wound on reels each with 21 take outs, stainless steel electrodes and cable jumpers and various connectors. The system is compatible with a portable PC-type computer. Operating power comes from an internal 12 volts rechargeable NiCd battery pack. Model section plotting of 1D and 2D model

interpretation sections in colour or gray scale including topography, reference data and reference levels, utility software for extraction of VES, data manipulation and conversion, graphical output in PCX-file format *etc.*, are also available (ABEM instruction manual, 2010).

The Lund ES 464 basic system include one ES464 field unit with clip-on NiCd rechargeable battery pack and one communication cable from electrode selector to Terrameter.

It is a method whereby consecutive readings are taken automatically and the results are averaged continuously. Signal Averaging System (SAS) results are more reliable than those obtained from single-short systems. The SAS 1000 can operate in different modes, *e.g.* resistivity, self-potential and induced polarization. In all its modes it is capable of measuring simultaneously in four channels thus making it suitable in all sorts of resistivity surveys. The SAS-EBA external 12 volts adapter allows the terrameter to utilize an external 12 volts D.C. source *e.g.*, a car battery. Stainless steel electrodes establish electric contact through long cables, to an ionic conductor which is the ground. All sort of electrodes generate “noise” (the fluctuating voltage that appears between a pair of electrodes placed so close that no other natural voltages appear). But stainless steel electrodes create less noise than electrodes made of ordinary steel. Current electrodes and potential electrodes make good contact with the ground to ensure low contact resistance and stability respectively (ABEM LUND Instruction Manual, 2010).

The cables incorporate heavy gauge conductors with excellent insulation to ensure good survey results. The cables are expandable for deeper penetration by connecting them in series with a cable joint. The cables have take-outs at 2m intervals along its length from

which they can be connected to the electrodes using cable jumpers having crocodile clips at both ends.



Plate 3.1: ABEM LUND Imaging system together with Terrameter SAS 4000 and ES 464.

3.2 Field Work

3.2.1 Reconnaissance Survey

A reconnaissance visit to the study area was done in order to familiarize with the community and also obtain valuable information about the area and its environs. G.P.S. coordinates and photographic images at specific locations were taken to further guide decision making.

3.2.2 Data Acquisition

Two dimensional (2D) electrical resistivity data were first acquired along a profile, designated as 'Test Profile'. The Test Profile was chosen to pass along a point with an exposed subsurface that reveals different layers, including that which is rich in cassiterite. The Wenner, Schlumberger and Dipole-Dipole electrode configurations were

used for data acquisition at the Test site to determine the most suitable resistivity array for the exploration of the subsurface layer that is rich in cassiterite within the area.

Data acquired at the test site were processed and interpreted, the result suggest Schlumberger array as the suitable configuration for exploration of cassiterite rich layers. Results at the test profiles and the reason for the choice of Schlumberger array are contained in chapter four and subsequence data were acquired along a total of Five Profiles (labeled Profile 1-5). Three Profiles (Profiles 1 to 3) were laid parallel to each other, 5 m apart while the other two, Profiles (4 and 5), were laid perpendicular to Profiles 1 to 3. Profile one, two and three are trending in the west-east direction and profile four and five trend in the north-south direction. The test profile is trending in the NE-SW direction (figure 3.1).

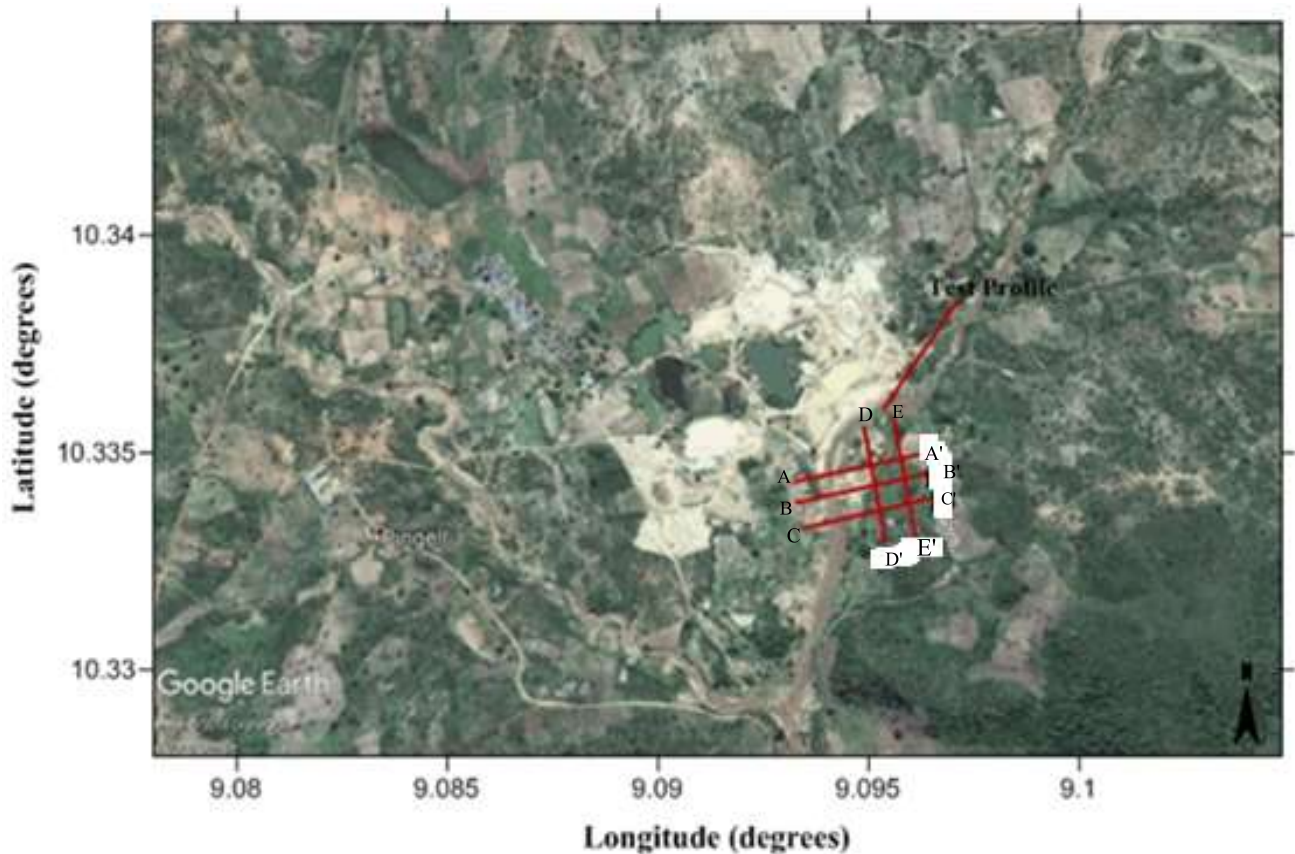


Figure 3.1: Profile Layout Superimposed on Google Earth Map (AA', BB', CC', DD' and EE' represents the start and end of each profiles respectively).

These profiles were taken by placing the stainless-steel electrode stakes into the ground at an interval of 5 meters each, along each profile. The Lund multi-cable was then laid on the ground and jumpers were used to connect the smart electrode to its electrode stake, making sure that there was an electrical contact between them. The switching off and on of the smart electrodes is controlled automatically by the electrode selector. The cable of electrode was then connected to the electrode selector. Also, the selector was connected to the multi-port of the Terrameter with a connecting cable and the details of the profile from which data is to be collected is entered into the Terrameter and be made ready for data collection. The actual measurement was carried out after the contact resistance test output

gives good result. Otherwise the causative electrodes will be checked properly if there may be need for reconnection or watering to enhance good contact. This same process was repeated for all 5 profiles. Figure 3.1 shows the profile layout on the study area.

Coordinates of end points of each profile were recorded using a GPS and the coordinates of profiles were noted (Table 3.1) for reference purpose.

Table 3.1: Coordinates of the beginning and end point of each profile.

Profile	Start Point	End Point
Test Profile	N10 ⁰ 20' 06.6" E 9 ⁰ 05' 45.1"	N10 ⁰ 20' 04.6" E 9 ⁰ 05' 43.2"
1	N10 ⁰ 20' 02.3" E 9 ⁰ 05' 41.9"	N10 ⁰ 20' 03.6" E 9 ⁰ 05' 42.6"
2	N10 ⁰ 20' 02.2" E 9 ⁰ 05' 42.2"	N10 ⁰ 20' 02.2" E 9 ⁰ 05' 42.1"
3	N10 ⁰ 20' 03.4" E 9 ⁰ 05' 42.8"	N10 ⁰ 20' 04.5" E 9 ⁰ 05' 43.6"
4	N10 ⁰ 20' 03.3" E 9 ⁰ 05' 43.3"	N10 ⁰ 20' 02.6" E 9 ⁰ 05' 42.9"
5	N10 ⁰ 20' 02.3" E 9 ⁰ 05' 42.5"	N10 ⁰ 20' 03.2" E 9 ⁰ 05' 43.0"

3.2.3 Field Problems

Some of the problems encountered during the field measurement are as follows:

- i. Draining of the battery during the field measurement slowed down the data acquisition process because the battery has to be recharged after some measurements were taken. Eventually, an alternative battery had to be provided which increased the field survey expenses.
- ii. Sometimes poor contact existed between the electrodes and ground when the electrodes were hammered vertically into the ground.
- iii. The practical difficulty in moving great length of cables and electrodes around was also very tasking.

3.3 Data Processing Procedure

The raw field data were processed using RES2DINV (Loke and Barker, 1996). This is a computer program that automatically determines a two-dimensional (2D) resistivity model for the subsurface for the data obtained from electrical survey. It is a window-based program.

The forward problem is solved through a finite difference algorithm, whose main features are a versatile user-defined discretization of the domain and a new approach to the solution of the inverse Fourier transform. The forward modelling subroutine is used to calculate the apparent resistivity values. The inverse procedure is based on an iterative smoothness-constrained least-squares algorithm. This computer program uses a smoothness constrained non-linear least-squares optimization inversion technique to convert measured apparent resistivity values to true resistivity values and plot them in cross-sections. The inversion process removes the geometrical effects from the pseudo section and produces an image of true depth and true formation resistivity. One advantage of this method is that the damping factor and flatness filter can be adjusted to suit different types of data. The program creates a resistivity cross-section, calculates the apparent resistivities for that cross-section, and compares the calculated apparent resistivities with the measured apparent resistivities. The iteration continues until a combined smoothness constrained objective function is minimized. The depth of investigation cannot be determined by simple calculations and it depends on the acquisition geometry, the conductivity structures and data errors (Oldenburg and Li, 1999). However, they have demonstrated through various modelling exercises that there is a loss of reliability in the inverted resistivity values at the bottom and ends of resistivity images where the resistivity values are least constrained by the data.

A common method for presentation of 2D resistivity data is the drawing of pseudo sections. A pseudo section is made by plotting the data points in a diagram, using the length axis for the distance along the surveying line and the depth axis for the electrode separations (ABEM LUND Instruction Manual, 2010). The distance for the electrode configuration midpoint is thus plotted against the electrode separation for each measured data point, letting the latter reflect the measurement depth. The corresponding apparent resistivities for the plotted points are then used to contour the variation in apparent resistivity along the surveying line. The pseudo section thus obtained reflects the variation of resistivity in the ground in a qualitative way, and approximate structures and depths to layer interfaces may be estimated. It should be noted that the pseudo section is simply a 2D equivalent of the plotted field data points in a linear depth scale. In this context, drawing of pseudo sections needs computer assistance to be practicable due to the large amount of data. The PSEUDO.EXE and ERIGRAPH.EXE software have been developed for automatic drawing of pseudo sections in grey scales or colors, using linear interpolation between data points (ABEM LUND Instruction Manual, 2010). Linear interpolation involves no smoothing of data, and hence gives a good indication of the data quality. Twelve different colors or grey levels are used for plotting data. Each data point used for drawing the pseudo section is indicated in the section by a dot. Presenting DC-resistivity data in color plots may be disputable as the data do not contain any spectral information. However, presenting D.C. resistivity data in color plots makes it easier to see the variations in resistivity. This is important because, small changes in resistivity in one part of a long profile may be significant even if there is a very large variation along the profile.

The 2D model used by the program divides the subsurface into a large number of rectangular blocks, to determine the resistivity of the rectangular blocks that will provide an apparent resistivity pseudo section that agrees with the actual measurements. Figure 3.2a shows an arrangement of the blocks loosely tied to the distribution of the data points in the pseudo section. The distribution and the size of the blocks are automatically generated by the program, so that the number of blocks, usually do not exceed the number of data points. The depth of the bottom row is set to be approximately equal to the median depth of investigation (Edwards, 1977) of the data points with the largest electrode spacing. Figure 3.2b shows an alternative arrangement with blocks of uniform width extending to the ends of the survey line.

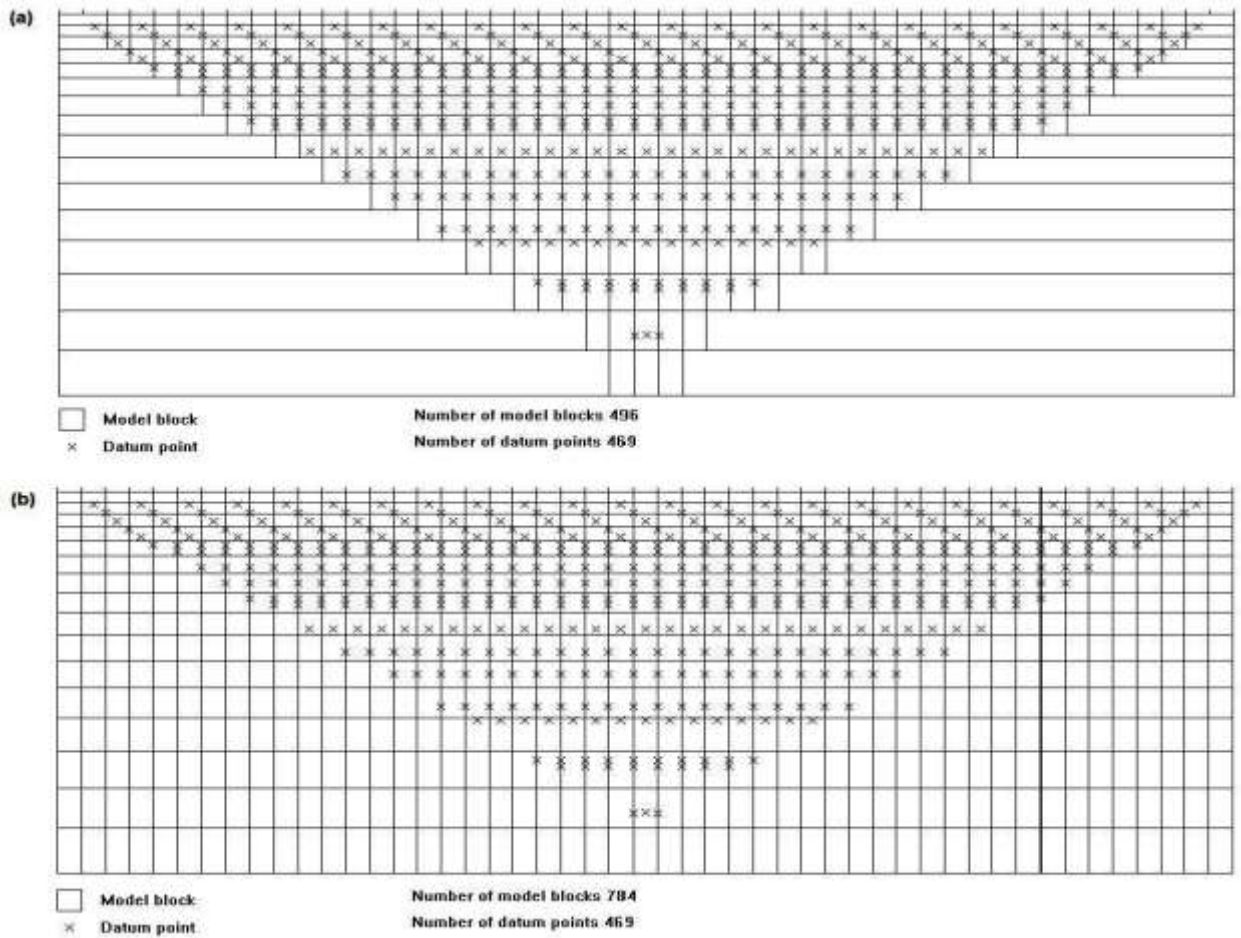


Figure 3.2: Two possible arrangements of the blocks used in a 2-D model together with the data points in the pseudo-section.

The RES2dinv program uses a forward modelling subroutine (smoothness-constraint method) to calculate apparent resistivity values and a non-linear least-squares optimization technique for the inversion routine. (deGroot-Hedlin and Constable, 1990). The optimization method basically tries to reduce the difference between the calculated and measured apparent resistivity values by adjusting the resistivity of the model blocks. A measure of this difference is given by the root-mean squared (RMS) error. However, the model with the lowest possible RMS error can sometimes show large and unrealistic

variations in the model resistivity values and may not always be the "best" model from a geological perspective. In general, the most prudent approach is to choose the model at the iteration after which the RMS error does not change significantly and usually occurs between the 3rd and 5th iterations.

The measured apparent resistivity data files for all the resistivity imaging survey lines were downloaded from the ABEM ES464 Terameter to a flash drive. The flash drive was uploaded into a computer in which ABEM file conversion (SAS4000 Utilities) and RES2DINV application software had been installed. The SAS4000 Utilities software was used to convert the original data file (in. s4k format) to the appropriate (.DAT format) input file readable by the inversion software RES2DINV. A total of seven files were converted. Each of the converted file represents a profile which has been imported into the Res2dinv program. It is worth noting that to get a good model, the data must be of equally good quality. Therefore, the apparent resistivity data when viewed as a profile plot showing each data level was edited by eliminating or removing inherent (bad) data points (example shown by Fig. 3.3). Even though great care was taken during the survey, inherent data points were visible by their unique too high or low too values when compared to neighboring data points. The bad data points might have been generated from sources such as; very poor ground contact at an electrode such that sufficient current cannot be injected into the ground, or failure of the relays at one of the electrodes. Eliminating these bad data points were inevitable, otherwise they might influence the final output model.

The inversion of the input data set for each profile was carried out (after satisfactory editing) with least-squares inversion routine. The final output displayed after the inversion

were the measured and calculated apparent resistivity pseudo sections and the inverse model showing true depth and true formation resistivity.

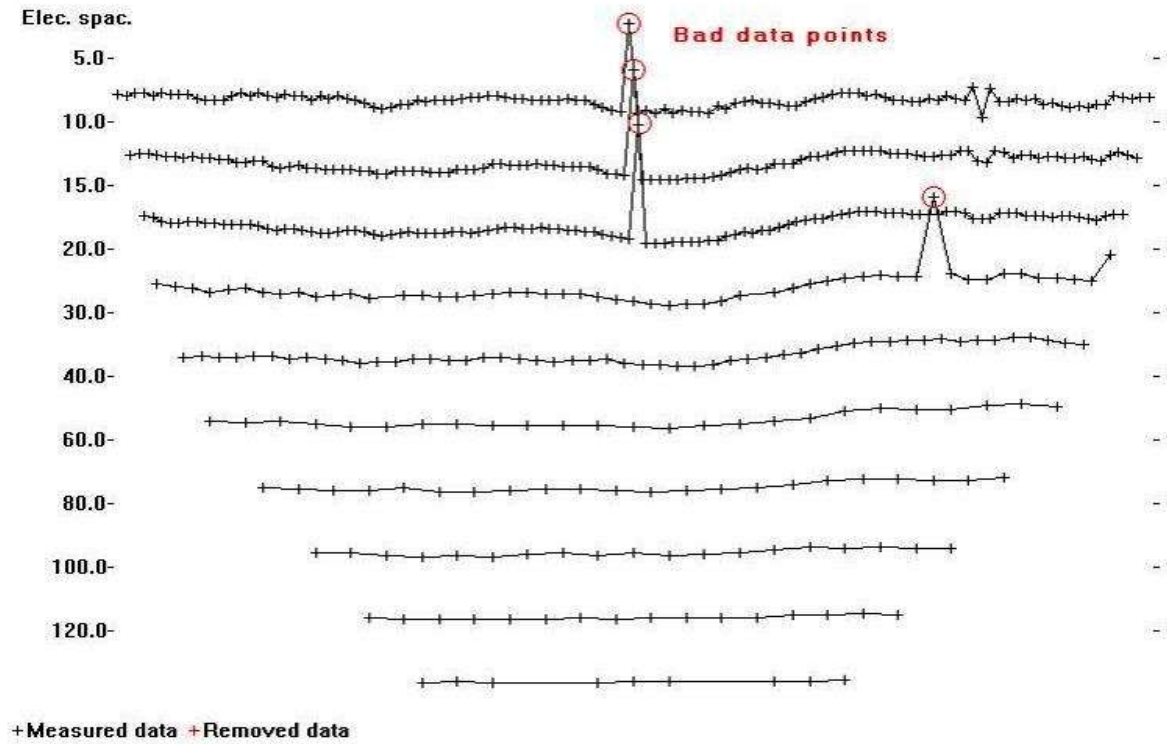


Figure 3.3 An example of a profile showing data set with a few bad data points.

CHAPTER FOUR

RESULTS AND INTERPRETATION

4.1 Lithological Log

Interpretation of geophysical data entails expressing information acquired from geophysical field measurements into a clear geological term. To obtain such geological results, available and reliable geological controls are necessary for a reliable interpretation of geophysical data. Such controls are often obtained from borehole data, results of previous works within such an area and a good knowledge of the geology of the area. Unfortunately, no borehole information and/or previous studies had been carried out within the area of study. However, a representative lithology of the area produced by using tape to measure depths to different lithology at an exposed mining pit (figure 4.1). The top soil comprises mainly of the overburden (laterite and clay), cassiterite bearing layer and the granitic rock.

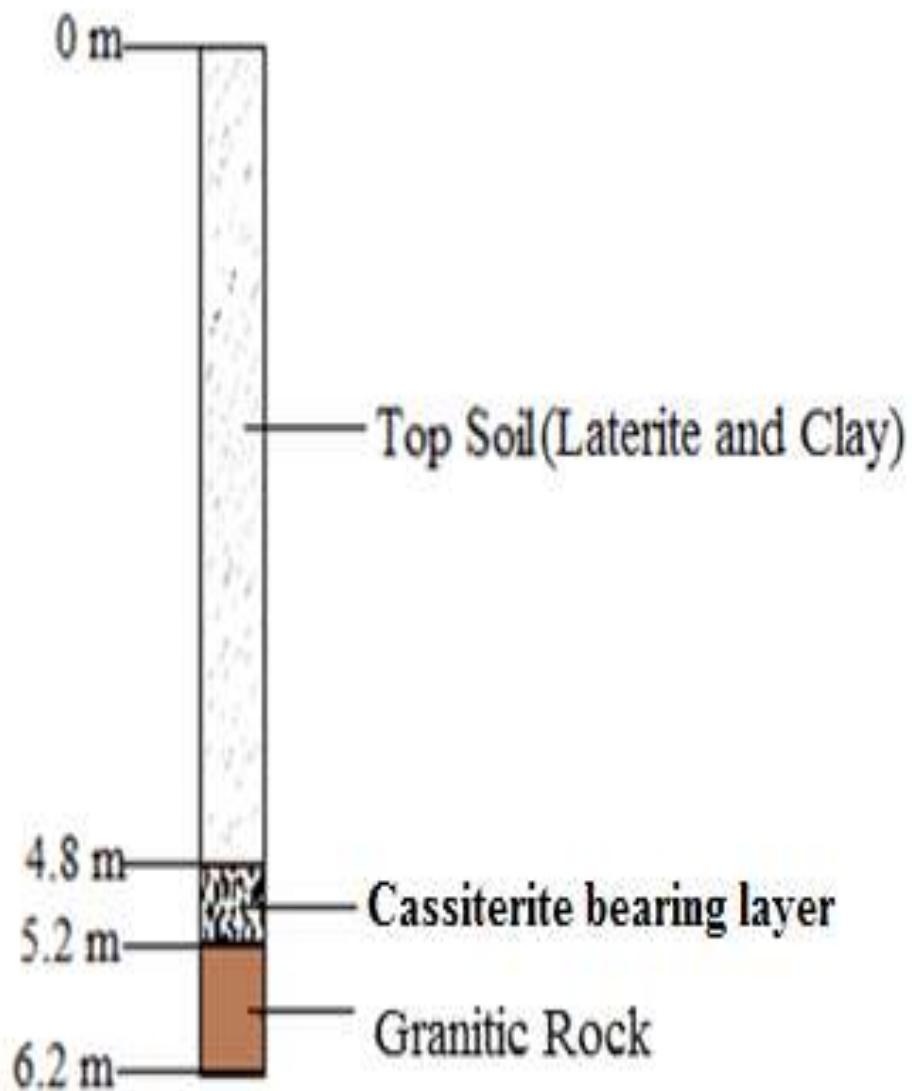


Figure 4.1: Section of exposed subsurface in study area.

Figure (4.2), inverse model of Schlumberger data, the resistivity of common rocks and minerals (Telford *et al.*, 1990; Akanbiet *et al.*, 2017) were used to draw the standard table (as seen in table 4.1), used to interpret the 2D electrical resistivity results.

Table 4.1: Standard resistivity values of rock materials (Telford *et al.*, 1990; Akanbiet *al.*, 2017).

S/N	Rock Type	Resistivity
1	Top soil (Laterite and clay)	1 – 50 Ωm
2	Cassiterite bearing layer	60 – 250 Ωm
3	Weathered basement	270 – 600 Ωm
4	Fresh Basement and granitic rock	➤ 600 Ωm

4.2 Inversion and Interpretation of 2D Model of ERT Data Acquired at Test Site

The result of the 2D electrical resistivity survey taken at the test site of the study area, are presented in Figures(4.2) to (4.4).

The results show three images for each 2D section and depict the images of the geoelectric sections obtained from the processed data. The upper image is a plot of the measured apparent resistivity pseudo-section, the middle image is the calculated apparent resistivity pseudo-section and the lower image is the resistivity model obtained after a definite number of iterations of the inversion program. The optimization method tries to reduce the difference between the calculated and measured apparent resistivity values by adjusting the resistivity of the model blocks. A measure of this difference is given by the root-mean-squared (RMS) error. The resistivity model shows variation in the geologic properties of the subsurface, which is in relation to the measured resistivity with scales shown at the lower end of each plot. The side bar shows the depth below the subsurface and the lateral distance is shown above the section.

Figures (4.2), (4.3) and (4.4) are respectively the 2D resistivity inversion model of the Test site using dipole-dipole, Wenner, and Schlumberger configurations. The section of exposed subsurface, which was dug at a lateral distance of 55 m along the profile, is posted on each inversion model. This is to show the correlation between the section and the inversion model.

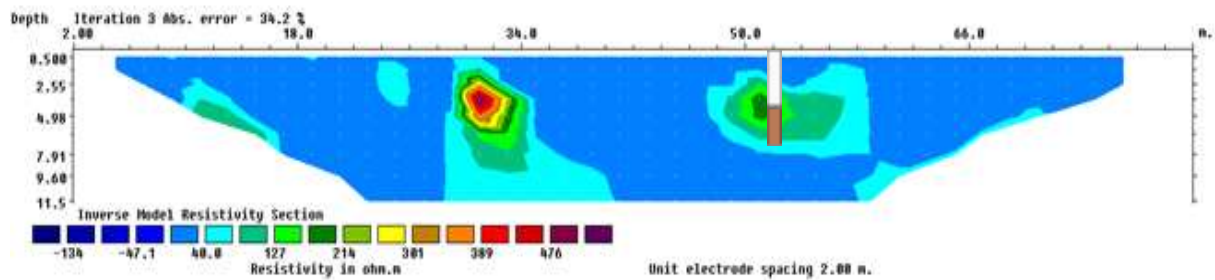


Figure 4.2: Result of 2D Inversion of the Dipole-Dipole array data with section of exposed subsurface along Test Profile.

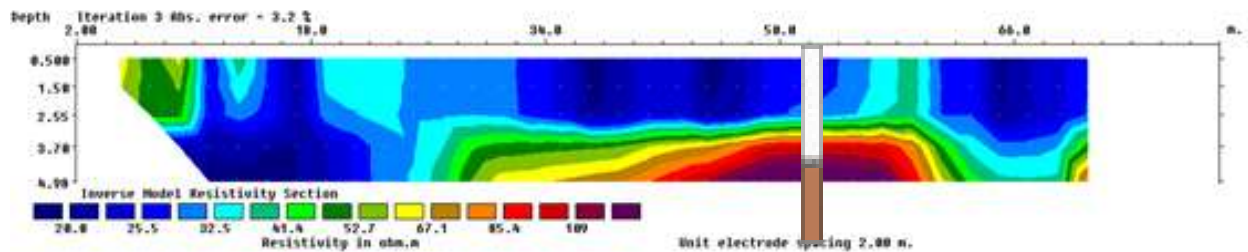


Figure 4.3: Result of 2D Inversion of the Wenner array data with section of exposed subsurface along Test Profile.

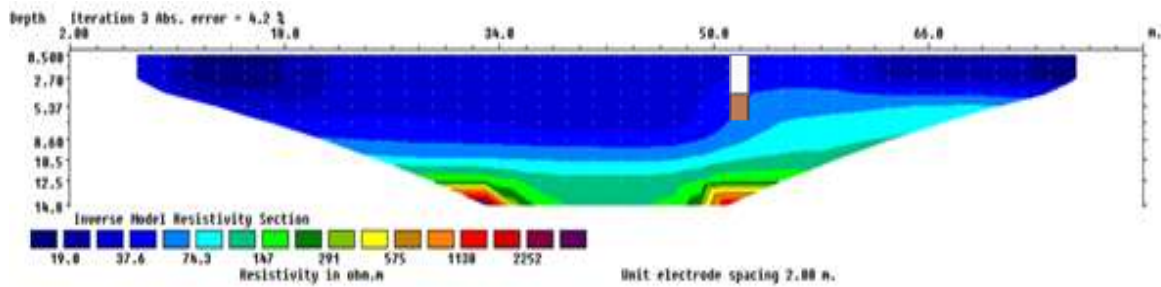


Figure 4.4: Result of 2D Inversion of the Schlumberger array data with section of exposed subsurface along Test Profile.

Based on the result gotten from the inversion model of the test site, the schlumberger array proved to be a better representation of the cassiterite bearing layers. This is because, the schlumberger array works well in layered earth i.e. gives a clearer depiction of the earth's lithology.

4.3 Inversion of Acquired 2D ERT Data

The data acquired along a total number of five profiles with schlumberger configuration was inverted using the RES2DINV software. The 2D electrical resistivity tomography of the earth's subsurface along the entire profiles are presented in Figures(4.5) to (4.9).

4.4.1 Result of Profile 1

Figure 4.5 shows the resistivity inversion tomography along Profile 1. Three layers can be clearly classified from the profile with the topsoil stretching laterally and extending to a depth between 3 m and 6 m. The resistivity value associated with the topsoil ranges from 19 Ω m to 70 Ω m. The low resistivity value may be due to the clayey nature of the topsoil. The second layer resistivity, and depth ranges between 75 Ω m and 140 Ω m, and 6 m and 12 m respectively. This is the layer which is rich in cassiterite. The third layer stretches beyond 12

m in depth with resistivity values above 800 Ωm . The resistivity of this layer is suggestive of the occurrence of the fresh basement.

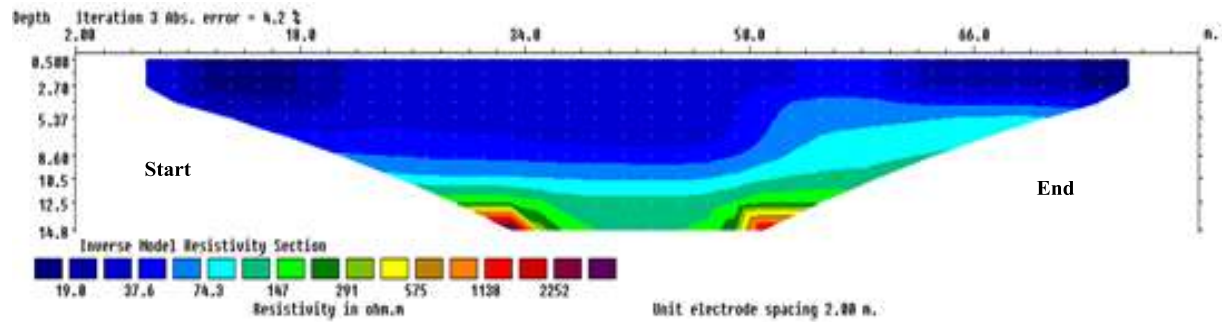


Figure 4.5: Result of 2D Inversion of the Schlumberger array data along Profile 1.

4.4.2 Result of Profile 2

Figure 4.6 is the resistivity inversion tomography along Profile 2. With the section of exposed subsurface as control, three geo-electric layers can be delineated. The topsoil extends to a depth approximately 5.37 m. The resistivity value associated with the topsoil along the second profile is generally lower than 32 Ωm . The low resistivity value may be due to the clayey nature of the topsoil. The second layer resistivity ranges between 60 Ωm and 150 Ωm and a depth range of 6 m and 12.5 m. The layer is interpreted as being rich in cassiterite. Below the Second layer is the third layer with resistivity generally greater than 300 Ωm and can be inferred to be associated with the fresh basement.

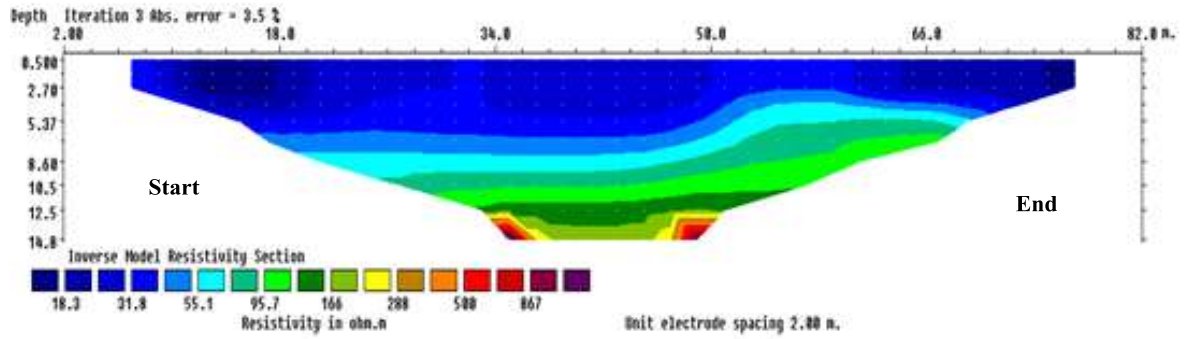


Figure 4.6: Result of 2D Inversion of the Schlumberger array data along Profile 2

4.4.3 Result of Profile 3

Figure 4.7 is the resistivity inversion tomography along Profile 3. From the inversion result, the resistivity values of the first layer are generally lower than 40 Ωm . The low resistivity nature is suspected to be due to the clayey nature of the soil and small cassiterite deposits. Along the profile, between 37 m to 50 m, there exists a weak zone with materials having resistivity between 128 Ωm to 240 Ωm and stretching downwards to form part of the second layer. This layer suspected to form the cassiterite bearing layer, having thickness of approximately 6 m. Below this layer is the fresh basement. It stretches beyond 13 m and has resistivity above 1,000 Ωm .

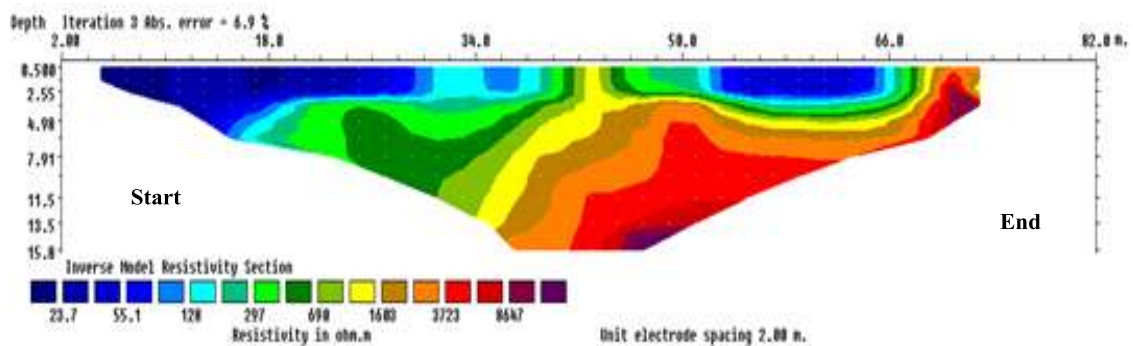


Figure 4.7: Result of 2D Inversion of the Schlumberger array data along Profile 3.

4.4.4 Result of Profile 4

Figure 4.8 is the resistivity inversion tomography along Profile 4. The first layer comprises of materials with resistivity generally below $400 \Omega\text{m}$ and are at an approximate depth of 2.5 m. The low resistivity nature is suspected to be due to the clayey nature of the soil and some cassiterite deposits. The Second layer is thin stretching laterally across the entire length of the profile. It has an approximate thickness of 1 m and resistivity range between $400 \Omega\text{m}$ to $1,500 \Omega\text{m}$. The layer suspected to form the weathered basement. Below this layer is the fresh basement comprising of highly resistive materials above $6,000 \Omega\text{m}$.

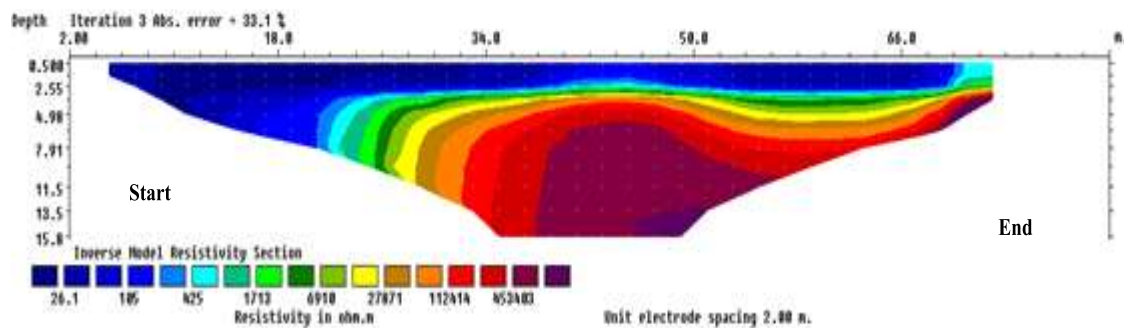


Figure 4.8: Result of 2D Inversion of the Schlumberger array data along Profile4.

4.4.5 Result of Profile 5

Figure 4.9 is the resistivity inversion tomography along Profile 5. The first layer comprises of materials with resistivity generally below $120 \Omega\text{m}$ at an approximate depth of 3.0 m. A weak zone exists along the profile (between 42 m to 48 m) and extends into the second layer. The Second layer is thin (below 1 m) and it extends laterally across the entire length of the profile. The resistivity range of the second layer is approximately between $124 \Omega\text{m}$ to $250 \Omega\text{m}$ and it's suspected to be cassiterite bearing layers (with a maximum depth of 10 m). The third layer comprises of highly resistive materials, with resistivity generally above

10,000 Ωm . This layer is at a depth of approximately 5 m and can be inferred to be the fresh basement.

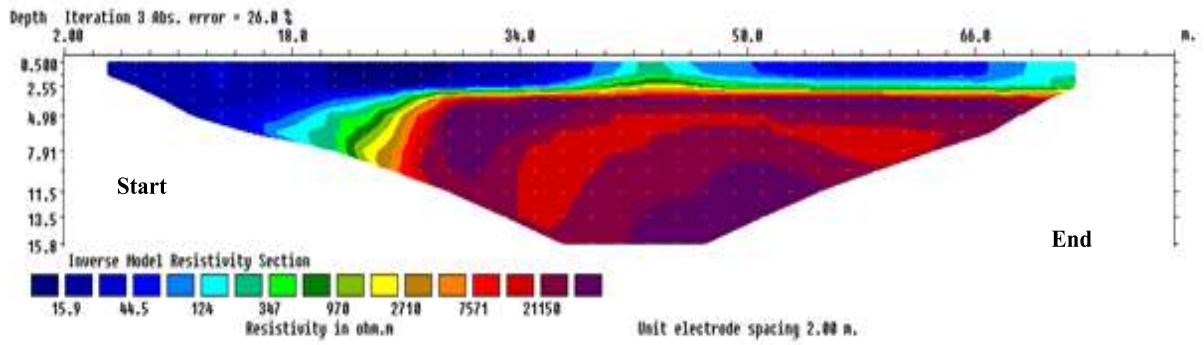


Figure 4.9: Result of 2D Inversion of the Schlumberger Array Data along Profile5.

Table 4.2 gives an overview of the profiles, showing the maximum and minimum resistivity and depth of each layer.

Profiles	Layers	Minimum Resistivity (ohm-m)	Maximum Resistivity (ohm-m)	Minimum Depth (m)	Maximum Depth (m)
1	Overburden	19	70	3	6
	Weathered	75	140	6	12
	Fresh Basement	500	>800	12	>12
2	Overburden	11	32	1	5
	Weathered	60	150	6	13
	Fresh Basement	300	>300	14	>14
3	Overburden	10	39	2	6
	Weathered			7	14
	Fresh Basement			15	>15
4	Overburden	10	300	1	3
	Weathered	400	1500	4	7
	Fresh Basement	1600	>6000	8	>10
5	Overburden	10	120	2	6
	Weathered	124	250	7	13
	Fresh Basement	1000	>6000	15	>15

Figure 4.10: shows the spatial display of all the 2D inverse resistivity models.

This display shows in a view, variations in the inferred lithology of the subsurface, irrespective of the orientation of the profiles.

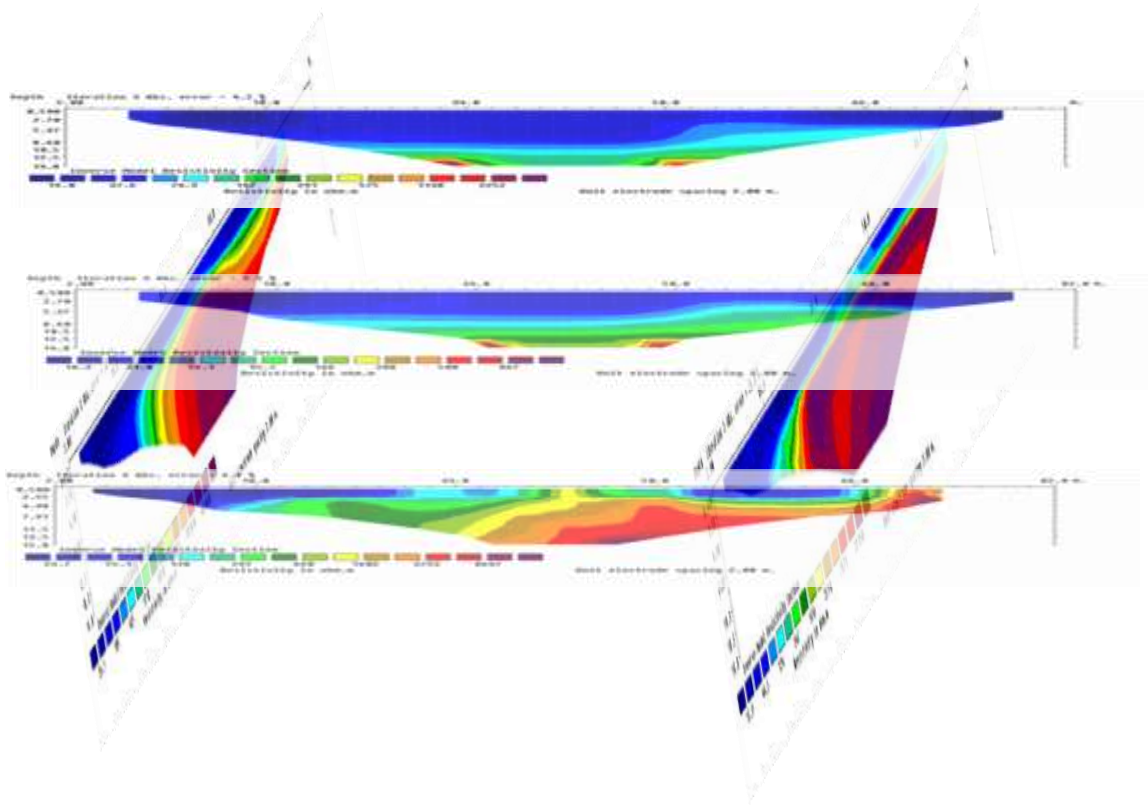


Figure 4.10: Spatial display of ERT of the study area.

Figure 4.11 gives the 3D horizontal slices that contained a total number of nine (9) layers with a maximum depth of 12 m and the absolute error obtained was 6%. This was obtained by collating the 2D profiles into one 3D file. Each layer of the slices gives the depth and resistivity contrast of the rock materials.

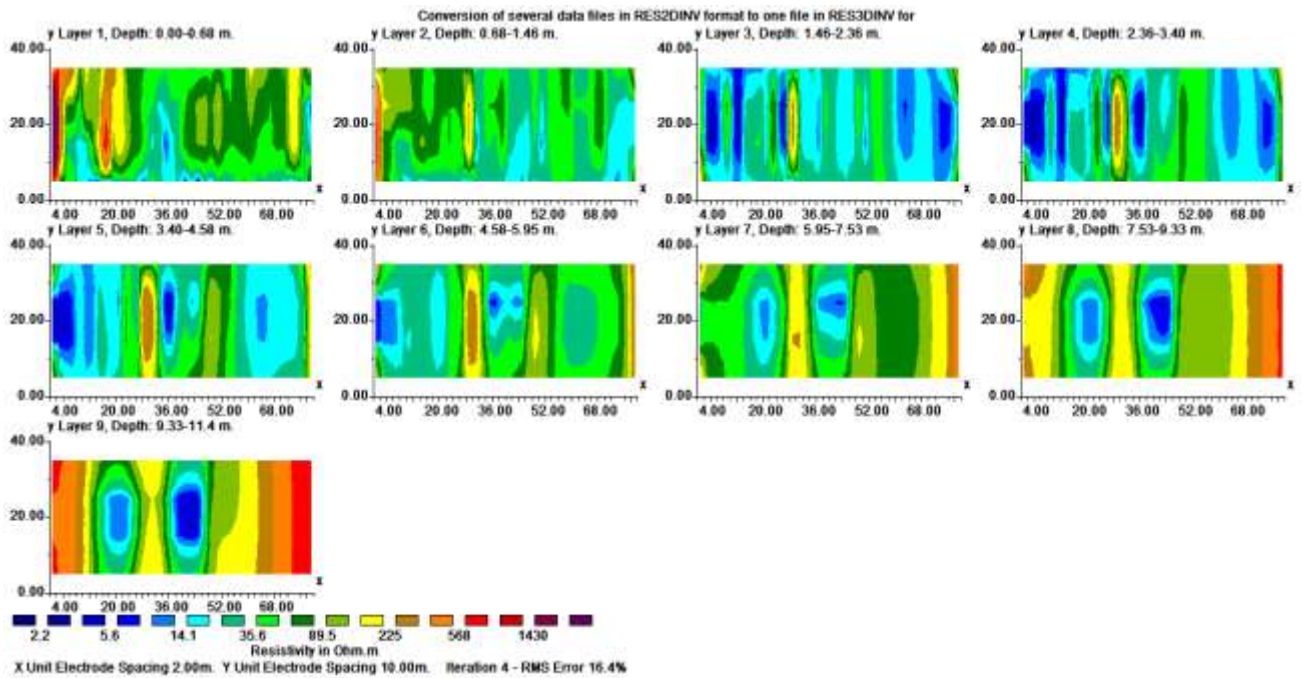


Figure 4.11: 3D horizontal depth slices of the subsurface with a grid size of 41x5.

CHAPTER FIVE

DISCUSSION, CONCLUSION AND RECOMMENDATION

5.1 Discussion

Lithological information and representative resistivity values of earth materials used in this study area in classifying the geologic layers were derived from Akanbiet *et al.*, 2017, and are as follows; 1 to 300 Ωm - overburden resistivity; 300 to 400 Ωm - weathered granite; 400 to 600 Ωm - cassiterite bearing layers; > 600 Ωm - granitic rocks and fresh basement. Cassiterite is dispersed in multitudinous, narrow greisen veins and quartz stringers in the roof zones of biotite granite intrusions, and usually entrapped within parent rock beneath an impermeable cover of roof rock dykes i.e. the biotite granite intrusions (Macleod *et al.*, 1971; Obaje, 2009). Erosion of these rocks over time would have rapidly uncovered some extensive area of cassiterite bearing granite and thus facilitate wide distribution of cassiterite in the surrounding drainage system.

The test site model was confirmed with a section of exposed subsurface dug 6.5 m along the profile. The section revealed some suspected cassiterite bearing layer on reaching a depth of 4.8 m. The lithology observed from the surface of the section to the depth of 6.5 m were reddish brown laterite and brown clayey sand (4.7 m thick); gravel mixed with alluvium and suspected cassiterite layer (1 m thick). The suspected cassiterite granules were confirmed to be cassiterite with dilute sulphuric acid in the presence of zinc. The test site profile revealed that the Schlumberger array configuration gives the best resolution of the cassiterite bearing layer. This is because the model of the Schlumberger array as compared to the dipole and Wenner arrays, gave a better resolution that conforms well with the

lithology of the section of exposed subsurface. The cassiterite bearing layer was found at the depth of 4.7 m, just as that of the section.

Two-dimensional electrical resistivity survey was then conducted within the unexplored/unexploited area of the Cassiterite mining site. Data was obtained along a total of five profiles using the Schlumberger array.

The result of the 2D electrical resistivity inversion reveals three to four layers in the surveyed area. The first layer (topsoil) consists of earth materials with resistivity values mostly less than 120 Ωm . This layer is inferred to consist of consolidated materials mainly clayey sand and laterite deposit in composition. It has an approximate thickness of 4.5m. The second layer has resistivity values ranging from 60 Ωm to 240 Ωm and may consist of weathered and fractured rocks with cassiterite composition at approximately 7.0 m deep.

The third layer is composed of highly resistive materials, generally greater than 800 Ωm , at depth stretching beyond 7 m. The high resistivity values in the third layer could be associated with the fresh basement.

Suspected igneous intrusions and fractures were observed within the subsurface along the profiles three and five. This suggests a possible relationship between these fractures and igneous intrusions. The probable depth to cassiterite bearing layer is 4 – 7 m, with resistivity range of 500 Ωm – 700 Ωm .

Considering profiles one, two and four, the probable depth to the cassiterite bearing layer is 4 – 7 m. Suspected igneous intrusions were also observed along these profiles, which could be dykes forming intrusion of biotite granites and cassiterite occurs only in association with biotite-granite.

5.2 Conclusion

Electrical resistivity imaging survey was successfully carried at the Cassiterite mining site in Pingel village, MagamaGumau, Bauchi State Nigeria with the aim of characterizing and delineating the extent of Cassiterite hosting structures.

The result of the 2D electrical imaging survey revealed that the Schlumberger array is the most suitable and reliable configuration for the exploration of Cassiterite.

The 2D electrical resistivity sections revealed suspected igneous intrusions and faults which are structures relevant to cassiterite mineralization. It also revealed the average depth to cassiterite bearing layer and to the basement.

The result further revealed the occurrence of four layered geoelectric sections within the study area. The top layer consists of low resistive materials, probably clay with mean thickness of 4.5m. The second layer, just below the top layer, is inferred to be the weathered basement, containing the cassiterite bearing layer. It consists of materials with varying resistivities between 50 Ωm to 250 Ωm at depth of approximately 6.0m. This layer is inferred to be the host for Cassiterite mineralization. The third layer is the fresh basement having resistivity values greater than 800 Ωm .

Based on the findings of this study, it can be concluded that there is presence of cassiterite potential at an average depth of 7m with resistivity range of 60 Ωm to 250 Ωm and if the mining activities are well coordinated, it can generate income for the rural dwellers as well as the state at large.

5.3 Recommendation

Based on the result of this study and also the physical properties of Cassiterite, such as high density, it is recommended that gravity survey be conducted in the area to further compliment the result herein.

REFERENCES

- ABEM Instrument A. B. (2010). Terrameter SAS1000/4000 LUND Imaging manual.
- Abdelwahab, H. (2013). Comparison of 2D and 3D Resistivity Imaging Methods in the Study of Shallow Subsurface Structures. *Greener Journal of Physical Sciences*. 3 (4), pp. 149-158
- Abubakar O.K, Sule, O.Y and Muraina, R. A. (2009) exploring the potential tailings of Bukurucassiterite deposit for the production of iron ore pellets. *Journal of minerals and characterization and engineering* vol. 8,5,PP. 359-361
- Ajakaiye DE (1983) Deep structures of alkaline ring complexes from geophysical data. In: Abstract, international conference on alkaline ring complexes in Africa. Zaria, Nigeria
- Akanbi, E.S, Ugodulunwa F.X.O and Gyang B.N (2012). Mapping Potential Cassiterite deposit at Naraguta area north central Nigeria using geophysics and geographic information system *Journal of mining and geology* volume 13, 21-26
- Akanbi, E.S, Ugodulunwa F.X.O and Gyang B.N (2017). 2-D Electrical Resistivity Survey for Cassiterite Potential Mapping in Jos-Bukuru Area, North Central, Nigeria. *Journal of Geography, Environment and Earth Science International* 10(1): 1-12
- Al Hameedami, M.A;2013. Comparison between different electrode arrays in delineating aquifer boundary by using 1D and 2D techniques in north Badra area eastern Iraq. MSc thesis Department of Geology, college of science, university of Baghdad, Iraq,142p.
- T. Balogun, The Changing Landscape of Jos, Nigeria. *Escape From America Magazine*9(11)Nov/Dec2007.http://www.escapeartist.com/efam/97/changing_landscape_of_Jos.html
- Beurlen H, da Silva MRR, Thomas R, Soares DR, Olivier P. (2008). Nb–Ta–(Ti–Sn) oxide mineral chemistry as tracer of Rare-Element Granitic Pegmatite fractionation in the Borborema Province, Northeastern Brazil. *Mineral. Deposita* 43: 207-228.
- Carlin JF. (2012) Tin: statistic and information. United states geological survey mineral commodity summaries, pp.170-171.
- Cowrie, A. (2010). Tin, an overlooked commodity. *The market oracle*, Aug, 19 2010. <http://www.marketoracle.co.uk>.
- Dada SS, Onema A, Rahaman A, Garba I. (2015). Lead reservoirs and metallization in Nigeria: Example of contrasting geological terrains. *J. Geosci. Geomatics* 3(2): 28-36. <https://doi.org/10.12691/jgg-3-2-1>.

- Dahlin, T. (1996). *2D resistivity surveying for environmental and engineering applications*. First Break. 14: 275-283.
- Dahlin, T. and Loke M.H.(1997). *Quasi-3D resistivity imaging-mapping of three-dimensional structures using two-dimensional DC resistivity techniques*. Proceedings of the 3rd Meeting of the Environ. Engineering Geophysics. Society. pp. 143-146.
- Dahlin, T. (2000). *Short Note on Electrode Charge-up Effects in DC Resistivity data Acquisition using multi-electrode Arrays*. Geophysical Prospecting, 48, pp.181-187.
- DeGroot-Hedlin, C. and Constable, S., 1990. Occam's inversion to generate smooth, two-dimensional models from magnetotelluric data. Geophysics, 55, 1613-1624.
- Edem GO, Ekwueme BN, Ephraim BE. (2015). Geochemical signatures and mineralization potentials of Precambrian pegmatites of Southern Obudu, Bamenda Massif, Southeastern Nigeria. Inter. J. Geophy. Geochem. 2(3): 53-67.
- Ero KA, Ekwueme BN. (2009). Mineralization of pegmatites in parts of the Oban Massif, Southeastern Nigeria: A preliminary analysis. Chinese J. Geochem. 28(2): 146-153.
- Falconer, J.D (1921). Nigeria Tin, its occurrence and Origin. Economic geology, 7, 542-546
- Falconer, J.D. and Raeburn, C. (1923). The northern Tin fields of Bauchi Province. Journal of African earth science, vol.3, 223 Geoscience Remote Sensing. <http://dx.doi.org/10.5772/57163>.
- Garba I. (2003). Geochemical discrimination of newly discovered rare metal-bearing and barren pegmatites in the Pan-African (600 + 150 Ma) Basement of Northern Nigeria. App. Earth Sci. Trans. Inst. Min. Metal. 13: 287-291.
- Gayus, N.L. (2004). Subsurface Investigation of the permanent Site of Federal College of Chemical and Leather Technology, Zaria using D.C. Resistivity Method. Unpublished M.Sc. Thesis, Physics Department, Ahmadu Bello University, Zaria.
- Griffiths, D.H. and Barker, R.D. (1993). Two dimensional resistivity imaging and modeling in areas of complex geology. Journal of Applied Geophysics, 29, 211-226.
- Hoover, D.B., Heran, W.D., and Hill, P.L.(1992).*The Geophysical Expression of Selected Mineral Deposit Models*: U.S. Geological Survey Open-file Report 92-557, 129 p.

- Ikpokonte, A. E. (1984). Gravity And Magnetic Studies Of The Sub-Basalt Cassiterite Deposit in Plateau State, Nigeria. M.Sc. Thesis, Ahmadu Bello University, Zaria
- Imeokparia EG. (2015). The Applied Geochemist and the Challenges of Georesource Evaluation for Sustainable Development and Environmental Management. Inaugural Lecture delivered at University of Benin, Benin City, Edo State, Nigeria.
- International Tin Research Institute Ltd. (ITRI Ltd). (2016). Report on Global Tin Resources & Reserves (security of long- term Tin supply).20.
- Jacobson, R. R. E. (1943). Report on Wolframite Investigation. Unpublished Geology Survey of Nigeria Report.Survey of Nigeria Bulletin, Vol. 17, 61pp.
- Keller, G. V. and Frischknecht, F.C. (1966); Electrical Methods in Geophysical Prospecting Pergamon Press, New York.
- Kinnaird JA, Nex PAM, Milani L. (2016). Tin in Africa. Episodes 39(2): 361-380. <https://doi.org/10.18814/epiiugs/2016/v39i2/95783>
- Kneisel C., Emmert A., and Kastl J. (2014). Application of 3D electrical resistivity imaging for mapping frozen ground conditions exemplified by three case studies. Geomorphology. DOI:10.1016/j.geomorph.2013.12.022
- Loke, M. H., (1999). *Electrical imaging surveys for environmental and engineering studies; A practical guide to 2-D and 3-D surveys*. Self-Published Note Book, 15-57.
- Matheis G, Emofurieta WO. (1990). The Older Tin province rare-metal pegmatite in Nigeria. Technical University of Berlin (West) Special Research Project on Arid Areas and University of Ife, Nigeria, 10.Milsom J. (2003). *Field Geophysics*.ThirdEdition.John Wiley and Sons Ltd.
- Matheis G. (1979). Geochemical exploration around the pegmaticSn-Nb-Ta mineralization of southwest Nigeria. Geol. Soc. Malaysia11:333-351
- Matheis G. (1987). Nigerian rare metal pegmatites and their lithological framework. J. Geol. 22: 271-291. <https://doi.org/10.1002/gj.3350220620>.
- Ministry of Mines and Steel Development (MMSD). (2012). Nigeria Mineral Projects. 36.
- Mohammed M. Al-Hameedawi and Jassim M. T.(2017). Comparison Between Four Electrode arrays in delineating sedimentary layers of alluvial fan deposits in eastern Iraq using 2D imaging technique. *springer –Verlag Germany*.
- Morteani G, Preinfalk C, Horn AH. (2000). Classification and mineralization potential of the pegmatites of the Eastern Brazilian Pegmatite Province. Mineral. Deposita 35: 638-655.

- Obaje N. G. (2009). *Geology and Mineral Resources of Nigeria*. Springer-Verlag Berlin Heidelberg.
- Oden MI, Igonor EE, Ukwang EE. (2013). Geochemical evaluation of the Pan-African pegmatites from parts of Oban massif, southeast Nigeria. *RMZ – M&G*. 60: 39-46.
- Ogunleye PO, Ike EC, Garba I. (2004). Multivariate statistical analysis of major and trace element data for niobium exploration in the Peralkaline Granites of the Anorogenic Ring-Complex Province of Nigeria. *Jour. Min. Geol.* 40(2): 107-117.
- Ogundipe IE, Obasi RA. (2016). Geology and mineralisation in the Albian Sediments of the Benue Trough, Nigeria. *British J. Earth Sci. Res.* 4(3): 1-15.
- Ogungbemi, O.S., Alu, O.O., and Ologe, O. (2014). Integrated Geophysical Approach to Solid Mineral Exploration: A Case Study of Kusa Mountain, IjeroEkiti, Southwestern Nigeria. *The Pacific Journal of Science and Technology*.15(1).
- Ogwuche, M.M. (2018). Application of Magnetics and Electrical Resistivity Methods for Exploration of Pegmatites at Saura Village, Keffi, Nasarawa State, Nigeria. Unpublished M.Sc. Thesis, Department of Physics, Ahmadu Bello University, Zaria.
- Okunlola OA. (2005). Metallogeny of Ta-Nb mineralization of Precambrian pegmatites of Nigeria. *Mineral Wealth* 137: 38-50.
- Okunlola OA. (2006). Regional metallogeny of rare metal (Ta-Nb) mineralization in Precambrian pegmatites of Nigeria. In: Oshin O. ed, *The Basement Complex of Nigeria and its Mineral Resources (A Tribute to Prof. M.A.O. Rahaman)*. Akin Jinad& Co. Ibadan, 107-126.
- Okunlola OA. (2008). Compositional trend in relation to Ta-Nb mineralization in the Precambrian Pegmatite of Aramoko-Ijero area, southwestern Nigeria. *J. Min. Geo.* 42(2): 113-126.
- Okunlola OA, Udoudo OB. Petrochemical Characteristics and Age of Rare Metal (Ta-Nb) Mineralization in Precambrian Pegmatites, Komu, Nigeria. *Int. Jour. Econ. & Environ. Geol.* 1(1): 21-26.
- Okunlola OA. (2017). Riches beneath our Feet: Mineral Endowment and Sustainable Development of Nigeria. Inaugural Lecture delivered at University of Ibadan, 92.
- Okpoli, C. C. (2013). Sensitivity and Resolution Capacity of Electrode Configurations. *International Journal of Geophysics* <http://dx.doi.org/10.1155/2013/608037>
- Olade, M.A. (1980). Geochemical characteristics of tin bearing and tin barren granites, northern Nigeria. *Economic geology* 75; 71-82. <http://doi.org/10.213/gsecongeo.75.1.71>

- Pastor, J. and Turaki, U. M. (1985). Primary Mineralization in Nigerian ring Complexes and its Economic Significance. *Journal of African Earth Sciences*. (3):pp 223-227.
- Resistivity Survey in Soil Science: A review, Soil Tillage Resistivity.83, pp. 173-193.
- Pratt, L.M., Comer JB, Brassell SC (1992) Geochemistry of organic matter in sediments and sedimentary rocks. SEPM Short Course 37:100 pp
- Saad,R.,Adli, and Mohamed, A.S.(2012). The Study of Iron Ore Prospect using 2-D Resistivity and Induced Polarization Method Electronic. *Journal of Geotechnical engineering*. vol.17.bund.v
- Samouëlian, A., Cousin, I., Tabbagh, A., Bruand, A. and Richard, G. (2005). *Electrical Resistivity Survey in Soil Science: A review, Soil Tillage Resistivity*.83, pp. 173-193.
- Sasaki, Y. (1992). *Resolution of resistivity tomography inferred from numerical simulation*. Geophysical Prospecting, 40, 453-464.
- Sudha, K., Israil, M, Mittal, S and Rai, J. (2009). Soil characterization using electrical resistivity tomography and geotechnical investigations. *Journal of Applied Geophysics* 67: 74–79
- Telford W.M., Geldart L.P. and Sheriff R.E. (1990). Applied Geophysics, Cambridge University Press.
- Umar, M., Ahmed, A.L., Magaji, S.S. and Bala, B. (2017). Electrical resistivity investigation of subsurface topography of RafinBareda drainage Basin as a tool for cassiterite- columbite exploration in Dutsen-Wai, Nigeria. *Bayero Journal of Pure and Applied Sciences*, 10(2):209-221.
- Umeshwar P. (2011). Economic Geology (Economic Mineral Deposits) 2nd ed. Cbs publishers and distributors, P.319
- Woakes M. (1988). Basement Metallogeny of Northwestern Nigeria. In: Oluyide PO,Mbonu WC, Ogezi AEO, et al, (eds). Precambrian Geology of Nigeria. Geological Survey of Nigeria, Kaduna, Nigeria, 183-194.
- Wright JB. (1970). Controls of mineralization in the older and younger tin fields of Nigeria. *Econ. Geol.* 51: 303-332.
- Wright JB. (1981). Review of the origin and evolution of the Benue Trough in Nigeria. *earth evol. Sci.* 1(2): 98-100